·Stephan Krohns[1] / Peter Lunkenheimer[1]

Ferroelectric polarization in multiferroics

[1] Experimental Physics V, University of Augsburg, Augsburg, Bayern, Germany, E-mail:
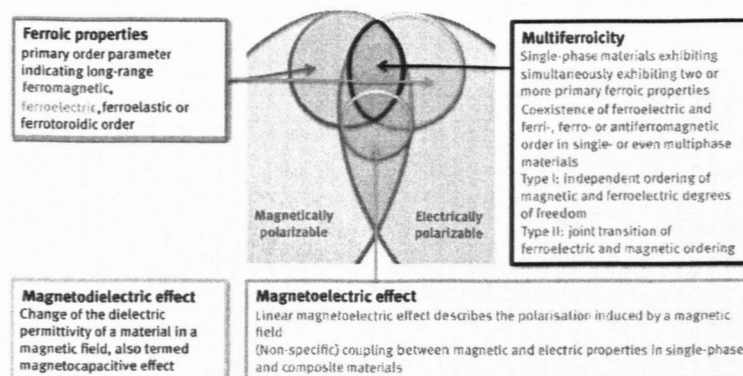stephan.krohns@physik.uni-augsburg.de

Abstract:
Multiferroic materials, showing ordering of both electrical and magnetic degrees of freedom, are promising candidates enabling the design of novel electronic devices. Various mechanisms ranging from geometrically or spin-driven improper ferroelectricity via lone-pairs, charge-order or -transfer support multiferroicity in single-phase or composite compounds. The search for materials showing these effects constitutes one of the most important research fields in solid-state physics during the last years, but scientific interest even traces back to the middle of the past century. Especially, a potentially strong coupling between spin and electric dipoles captured the interest to control via an electric field the magnetization or via a magnetic field the electric polarization. This would imply a promising route for novel electronics. Here, we provide a review about the dielectric and ferroelectric properties of various multiferroic systems ranging from type I multiferroics, in which magnetic and ferroelectric order develop almost independently of each other, to type II multiferroics, which exhibit strong coupling of magnetic and ferroelectric ordering. We thoroughly discuss the dielectric signatures of the ferroelectric polarization for $BiFeO_3$, Fe_3O_4, $DyMnO_3$ and an organic charge-transfer salt as well as show electric-field poling studies for the hexagonal manganites and a spin-spiral system $LiCuVO_4$.

Keywords: multiferroics, ferroelectrics, dielectric spectroscopy, polarisation measurements

DOI: 10.1515/psr-2019-0015

1 Introduction

The control of the ferroelectric polarization of multiferroic materials allows innovative magnetoelectric functionalities on a macroscopic as well as on a microscopic level, which may pave the way for next-generation building blocks for future electronic products [1–6]. Therefore, the analysis of the electrical and, hence, the ferroelectric properties is of key relevance. The objective of this manuscript is to gain fundamental insights into the underlying complex coupling mechanisms as well as a target-oriented manipulation of the magnetoelectric effect or the multiferroic ordering. Figure 1 provides a brief overview (adapted from Refs. [3] and [4]) on the definition of "multiferroicity" as well as "ferroic properties", "magnetodielectric effect" and "magnetoelectric effect". As there are various mechanisms giving rise to multiferroicity, we review dielectric and electric-field poling studies for six magnetoelectric and multiferroic materials based on five different and important underlying mechanisms: Lone-pair multiferroicity, geometrically driven improper ferroelectricity, relaxor-ferroelectricity in magnetic materials, electric-dipole-driven magnetism and strongly coupled spin-driven improper ferroelectricity.

Ferroic properties
primary order parameter indicating long-range ferromagnetic, ferroelectric, ferroelastic or ferrotoroidic order

Multiferroicity
Single-phase materials exhibiting simultaneously exhibiting two or more primary ferroic properties
Coexistence of ferroelectric and ferri-, ferro- or antiferromagnetic order in single- or even multiphase materials
Type I: independent ordering of magnetic and ferroelectric degrees of freedom
Type II: joint transition of ferroelectric and magnetic ordering

Magnetically polarizable   Electrically polarizable

Magnetodielectric effect
Change of the dielectric permittivity of a material in a magnetic field, also termed magnetocapacitive effect

Magnetoelectric effect
Linear magnetoelectric effect describes the polarisation induced by a magnetic field
(Non-specific) coupling between magnetic and electric properties in single-phase and composite materials

Figure 1: Definitions in the field of multiferroics (adapted from Ref. [4]) and the relationship between originally defined multiferroic and magnetoelectric materials (adapted from Ref. [3]). Ferroic order, especially ferromagnetism (ferroelectricity), forms a subset of magnetically (electrically) polarizable materials. In their intersection, multiferroic and magnetoelectric coupling can arise. For multiferroicity and the magnetoelectric effect the originally (blue) used and nowadays (red) commonly accepted definitions are given. The latter would lead to an enlarged intersection as e.g. antiferromagnetic order is also allowed for multiferroicity.

After an introduction on the signatures of ferroelectricity in dielectric spectroscopy and polarization measurements, we explicitly focus on the ferroelectric polarization of the following multiferroics:

Probably the most investigated single-phase multiferroic system is $BiFeO_3$ [7], which is indeed of particular interest for multiferroic applications as its multiferroicity already exists at ambient temperatures. We briefly review the dielectric and polar properties, only focusing on single crystals.

Magnetite is one of the oldest known magnetic materials. We discuss its fascinating property, namely relaxor-ferroelectricity, making Fe_3O_4 multiferroic [8]. However, the coupling of its order parameters is rather weak and occurs at temperatures below liquid nitrogen.

Electric-field poling studies of improper ferroelectrics like $YMnO_3$ and $ErMnO_3$ are rare [9–12]. Beside their multiferroic properties, these systems are in the scientific focus as they exhibit versatile ferroelectric domain and domain-wall properties [6]. Results of dielectric spectroscopy and polarization measurements combined with local-probe analysis allow manipulating the local structure via electric field and may pave the way towards their utilization in domain-wall-based electronics (as discussed, e.g. in DOI:10.1515/PSR.2019.0014).

A more exotic class of multiferroic materials is charge-transfer salts, which can exhibit improper ferroelectric ordering due to the localization of charges at organic molecules. For κ-$(BEDT$-$TTF)_2Cu[N(CN)_2]Cl$ (here BEDT-TTF stands for bis(ethylenedithio)-tetrathiafulvalene, often also abbreviated as ET), charge-order-driven electronic ferroelectricity was reported representing a novel type of multiferroic mechanism [13]. This allows in principle to tune magnetic ordering via an electric field, making this material class highly interesting from a fundamental point of view.

In multiferroics, the magnetic and ferroelectric order can develop almost independently from each other (i.e. type I). In contrast, type II multiferroics exhibit strong coupling of their ferroic orders [14]. Often complex magnetic ordering triggers improper ferroelectricity in these systems leading to identical ferroelectric and magnetic transition temperatures. For various compounds, like $TbMnO_3$ [15], $DyMnO_3$ [16] or $LiCuVO_4$ [17], the ferroelectric polarization can be controlled by magnetic fields. However, the reversed control is a challenge. For spin spirals (as discussed in DOI:10.1515/PSR.2019.0016), it was demonstrated that an electric field can change the helicity of these spirals from counterclockwise to clockwise rotation and vice versa [18–20]. Here, we briefly review the dielectric properties arising at the joint transition temperatures of $DyMnO_3$ [16].

Another prime example for a strongly coupled multiferroic is the spin-spiral system $LiCuVO_4$ [17]. We discuss its dielectric as well as its switching properties by electric fields and the impact of switching on the spin spirals.

2 Signatures of ferroelectricity

2.1 Signatures of ferroelectricity in dielectric spectroscopy

For multiferroics, due to conductivity contributions and/or extrinsic Maxwell–Wagner (MW) like relaxation phenomena arising from thin insulating barrier layers [21], it is often difficult or even impossible to unequivocally identify a polar ground state by a direct measurement of the electrical polarization. Therefore, one of the most prominent experimental methods used to identify ferroelectricity in multiferroics is dielectric spectroscopy. It allows for the detection of the significant anomalies in the temperature dependence of the real part of the dielectric permittivity (the dielectric constant ε') that are expected to occur at ferroelectric transitions. In this section, we discuss the typical experimental signatures of ferroelectricity in dielectric spectroscopy for the different classes of ferroelectric states, which in principle can also be found in multiferroics, e.g. $TbMnO_3$ (Ref. [15]) or $LiCuVO_4$ (Ref. [17]). For more details, we refer the reader to various review articles and books on ferroelectricity [22–26].

An important class of ferroelectric materials is constituted by the so-called displacive ferroelectrics. At their ferroelectric transition, a high-symmetry structure without permanent dipole moments transfers into a lower-symmetry structure with polar order. The latter arises from permanent dipole moments generated by local shifts of ions. In fact, in displacive ferroelectrics a so-called soft mode occurs, a dipolar-active transverse optical phonon that becomes soft when approaching the critical temperature. This finally results in the freezing-in of the long-wavelength ionic displacements and leads to an off-symmetry position of the involved ions that

˙establishes long-range polar order. An important property of displacive ferroelectrics is the divergence of the static dielectric constant ε_s: In the paraelectric phase, above the ferroelectric transition at T_{FE}, the temperature dependence of ε_s can usually be well described by a Curie–Weiss law.

$$\varepsilon_s = C / (T - T_{CW}).$$ (1)

Here C is the Curie constant determined by the dipole number per volume and the dipole moment and T_{CW} denotes the Curie–Weiss temperature, depending on the average interaction strength between the dipoles. Often the Curie–Weiss temperature and the ferroelectric ordering temperature are of similar order. Figure 2(a) schematically indicates $\varepsilon'(T)$ for a displacive ferroelectric. Below the transition temperature, $\varepsilon'(T)$ decreases again, leading to a sharp peak at T_{FE}. The detailed shape of this peak depends on the details of the transition, especially its first- or second-order nature [25, 26]. When performing conventional dielectric spectroscopy, typically covering frequencies in the Hz–MHz range, usually no significant frequency dependence of ε' is observed for this class of ferroelectrics.
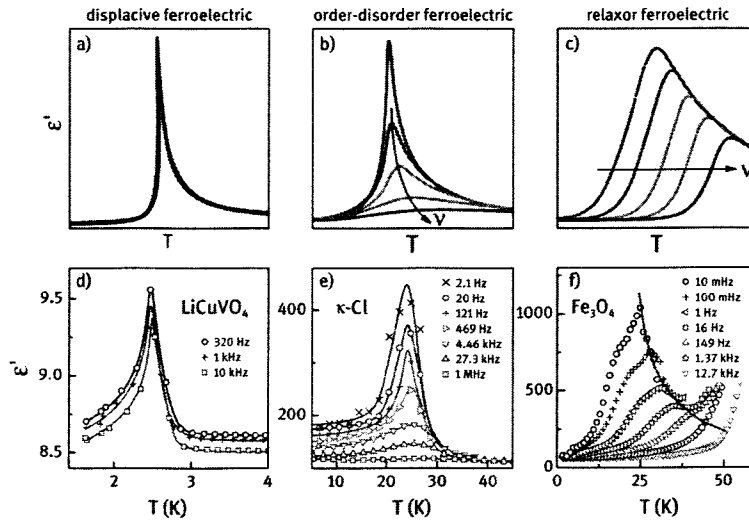

Figure 2: (a)–(c) Schematic plots of the temperature dependence of the dielectric constant of materials belonging to the three classes of ferroelectrics as typically detected by dielectric spectroscopy. The different lines represent $\varepsilon'(T)$ at different frequencies. Frames (d)–(f) show $\varepsilon'(\nu)$ of three multiferroics (LiCuVO$_4$ [27], κ-(BEDT-TTF)$_2$Cu[N(CN)$_2$]Cl [13] and Fe$_3$O$_4$ [8], respectively), which represent experimental examples corresponding to frames (a)–(c).

Figure 2(d) shows a multiferroic example of this type or ferroelectric, LiCuVO$_4$ [27]. It should be noted that this is an improper ferroelectric, where the polar order is driven by complex magnetic ordering via the inverse Dzyaloshinskii–Moriya interaction (see Section 3.6 for details on this material). However, this mechanism also leads to ionic displacements, which finally generates ferroelectricity. As documented in Figure 2(d), there is a small frequency dependence of ε' in this material, which may arise from the non-canonical origin of its polar order. However, it is much weaker than in the other two examples (Figure 2(e) and Figure 2(f)), which belong to different classes of ferroelectric as explained below.

While displacive ferroelectrics have no permanent dipole moments in their high-temperature paraelectric phase, in another class of ferroelectrics permanent dipole moments already exist above T_{FE}. In these so-called order–disorder ferroelectrics, in the paraelectric state these dipoles are statistically disordered with respect to site and time, but at the ferroelectric transition they align and polar order arises. Their temperature-dependent dielectric constant also exhibits a peak at the transition. However, in contrast to displacive ferroelectric, it also often reveals significant dispersion effects at audio and radio frequencies exhibiting the signatures of dielectric relaxation. This results from dipolar reorientations within double- or multi-well potentials, which slow down on decreasing temperature. In most cases, the detected dielectric response is almost monodispersive and approximately of Debye type, implying a single, well-defined relaxation time. In the paraelectric state, the dipolar units undergo fast reorientations between equivalent directions, while they reveal long-range order within the ferroelectric state. A schematic plot of the typical dielectric behaviour of displacive ferroelectrics is shown in Figure 2(b). While at low frequencies a well-defined and sharp peak arises in $\varepsilon'(T)$, it successively becomes suppressed with increasing frequency. Finally, almost no dielectric anomaly is detected at high frequencies, an effect that can occur in the kHz to MHz frequency range, depending on the material [26]. At low frequencies, only a small shift of the maxima in $\varepsilon'(T)$ is observed for different frequencies. Often the temperature dependence

3

`of the relaxation time determined from an evaluation of the frequency dependence of ε' and of the dielectric loss ε'' does not follow simple thermally activated Arrhenius behaviour. Instead, critical behaviour $\tau \propto 1/(T - T_c)^\gamma$ is frequently observed [26].

An example of a multiferroic exhibiting order–disorder ferroelectricity is provided in Figure 2(e). It shows $\varepsilon'(T)$ of the antiferromagnetic quasi-two-dimensional organic charge-transfer salt κ-(BEDT-TTF)$_2$Cu[N(CN)$_2$]Cl (κ-Cl) for several frequencies [13]. The strong suppression of the ferroelectric peak at high frequencies with only weak temperature shift, which is typical for order–disorder ferroelectrics (Figure 2(b)), is well documented. In this material, which will be discussed in more detail in Section 3.4, a combination of molecular dimerization and charge order leads to electronic ferroelectricity [13]. Above the charge-order transition, holes fluctuating within the dimers correspond to disordered dipoles, which finally order ferroelectrically below the transition.

The third class of polar materials treated here are the relaxor-ferroelectrics, which roughly can be regarded as ferroelectrics with a smeared-out phase transition (for reviews on these materials, see Refs. [28] and [29]). Often disorder helps promoting relaxor-ferroelectric states, which frequently is observed in solid solutions like the pseudo-cubic perovskite PbMg$_{1/3}$Nb$_{2/3}$O$_3$ [30]. Just as in the other classes of ferroelectrics, $\varepsilon'(T)$ of relaxors reveals a peak, however, with a smoothly rounded shape. Strong dispersion effects show up, which, especially in the frequency dependence of ε' and ε'', are reminiscent of the relaxation dynamics in glass-forming dipolar liquids as glycerol [31]. As indicated in the schematic plot in Figure 2(c), with increasing frequency the smeared-out ε'-peak shifts to higher temperatures and its amplitude becomes reduced. This results in characteristic dispersion effects below the peak temperatures. In relaxor-ferroelectrics, the observed shift of the peak temperatures in $\varepsilon'(T)$ usually signifies a Vogel–Fulcher–Tammann (VFT) law of the relaxation time $\tau(T)$ [32–34]:

$$\tau = \tau_0 \exp\left[\frac{B}{T - T_{VF}} \right] \tag{2}$$

Here, T_{VFT} is the divergence temperature of τ, where the dipolar dynamics finally becomes frozen, and B is an empirical constant. The temperature in eq. (2) represents the peak temperature in $\varepsilon'(T)$ and the relaxation time is deduced via $\tau = 1/(2\pi\nu)$, where ν is the frequency of the applied ac field. It should be noted that VFT behaviour is also found for the characteristic slowing down of molecular motion in glass-forming materials [31, 35]. The finding of a VFT law in relaxor-ferroelectrics usually is interpreted as being due to the glasslike freezing-in of short-range cluster-like ferroelectric order, assumed to exist in these materials [26, 28].

In most cases, the relaxation effects found in the dielectric spectra of relaxor-ferroelectrics do not show the characteristics of a simple monodispersive Debye relaxation. For the latter, the frequency dependence of the complex dielectric constant $\varepsilon^* = \varepsilon' - i\varepsilon''$ should behave like $\varepsilon^* = \varepsilon_\infty + (\varepsilon_s - \varepsilon_\infty)/(1 + i\omega\tau)$ with ε_∞ the high-frequency limit of ε' and $\omega = 2\pi\nu$. This leads to peaks in the dielectric-loss spectra with half widths of about 1.14 decades. However, in relaxor-ferroelectric, just like in most conventional glass-forming systems [31, 36, 37], the experimentally measured peaks are broadened. Various empirical functions are available to describe such broadened relaxation features in the dielectric spectra [38–40]. The broadening can be ascribed to a distribution of relaxation times arising from disorder [36, 37]. Usually, the occurrence of nano-scale ferroelectric clusters is assumed to explain the observed effects, in contrast to the macroscopic long-range ferroelectric domains existing in conventional ferroelectric states.

Finally, it should be noted that in relaxor-ferroelectrics, for temperatures above the dielectric-constant maximum, $\varepsilon'(T)$ often deviates from the characteristic Curie–Weiss behaviour, eq. (1), commonly found for conventional ferroelectrics. These deviations may arise due to short-range correlations between the mentioned nano-scale ferroelectric regions which are the precursors of the freezing-in of polarization fluctuations into a glasslike low-temperature state [41].

In Figure 2(f), we show an example of a multiferroic relaxor-ferroelectric, Fe$_3$O$_4$ [8]. It exhibits a stronger shift of the $\varepsilon'(T)$ peak with frequency than in the order–disorder system κ-Cl (Figure 2(e)) [13] and a broader, smeared-out peak. The ferroelectricity in this material is assumed to be driven by charge order [42], but the reason for the observed relaxor behaviour is not finally clarified. In Section 3.3, we provide a more detailed discussion of this material.

One should be aware that semiconducting single crystals or ceramics as well as electrically heterogeneous media often show a barrier-layer capacitance, which can be of internal or external origin [21]. Examples for internal layers are grain boundaries in polycrystalline samples. External layers are usually formed at the sample surface, e.g. by the formation of Schottky diodes when applying metallic contacts to a semiconducting material. This can lead to so-called MW relaxations, non-intrinsic effects that should not be confused with the intrinsic relaxational response found in order–disorder or relaxor-ferroelectrics. MW relaxations are caused by the presence of thin insulating barrier layers within the sample that give rise to high capacitances. The latter can lead to very high, so-called "colossal" [43], dielectric constants, which can impede the detection of an underlying ferroelectric ordering. These layers cause the artificial occurrence of a strong relaxation-like frequency-dependence

4

•of the dielectric properties, even without the presence of intrinsic relaxations in the investigated material. This can be understood when modelling the thin interface regions and the bulk sample by an appropriate equivalent circuit [21, 44]. Usually, at low frequencies the high capacitance of the layers dominates, leading to colossal dielectric constants, while at high frequencies the layer capacitors become shorted and the intrinsic properties may be detected. However, often intrinsic and non-intrinsic effect superimpose, hampering an unequivocal evaluation of the experimental data. In addition, these layers often show non-linear dielectric response (e.g. the Schottky diodes mentioned above), artificially mimicking ferroelectric hysteresis loop-like behaviour [45, 46].

Overall, great care should be taken to avoid MW effects leading to an erroneous claim of ferroelectricity or even multiferroicity. A prime example for a material showing MW relaxation due to internal and external barrier layer capacitances is $CaCu_3Ti_4O_{12}$ [47–49]. In this context, one should also mention $LuFe_2O_4$, which is often considered as a multiferroic with charge-order-driven polar order, i.e. electronic ferroelectricity [50]. However, the intrinsic nature of the detected dielectric properties of $LuFe_2O_4$ was questioned by several works, and non-intrinsic MW effects in this material seem very likely [51–53].

2.2 Signatures of ferroelectricity in polarization measurements

Polarization measurements are the most direct way to detect ferroelectricity in bulk materials. In the light of possible non-intrinsic contributions due to MW effects, a detailed dielectric analysis is advisable to deduce the temperature and frequency range as well as the electrical excitation fields, in which electric-field poling studies can be successfully performed. Positive-up-negative-down (PUND) measurements accompanying the hysteresis loop measurements can in addition verify the intrinsic nature of the detected polarization response [54].

Hysteresis loop measurements, for which the polarization P is measured in dependence of an external electric field E, represent the standard method for identifying ferroelectricity. This should lead to a clear hysteresis loop as schematically shown in Figure 3(a), which evidences the switchability of the polarization. It should be noted that, aside of the occurrence of a unique polar axis in the material, this switchability is an important characteristic of ferroelectrics. It essentially corresponds to domain nucleation, domain growth and the shifting of ferroelectric domain walls by the applied electrical field [26]. One should be aware that, at temperatures far below the ferroelectric transition, the domains often can be quite large and a possible domain-wall motion cannot by achieved by electrical fields of realistic amplitude (less than the breakdown field) [23–26, 54]. Therefore, $P(E)$ measurements at higher temperatures, shortly below T_{FE}, often are desirable. However, at elevated temperatures Ohmic losses due to mobile charge carriers, leading to finite dc conductivity, can dominate the measured hysteresis loops, hampering the detection of switchability. Moreover, as mentioned above, non-intrinsic effects, e.g. Schottky diodes arising at the contact-sample interfaces, can lead to considerable non-linear response of the sample to an applied electrical field, which can give rise to apparent $P(E)$ hysteresis loops, not related to ferroelectric switching [46].
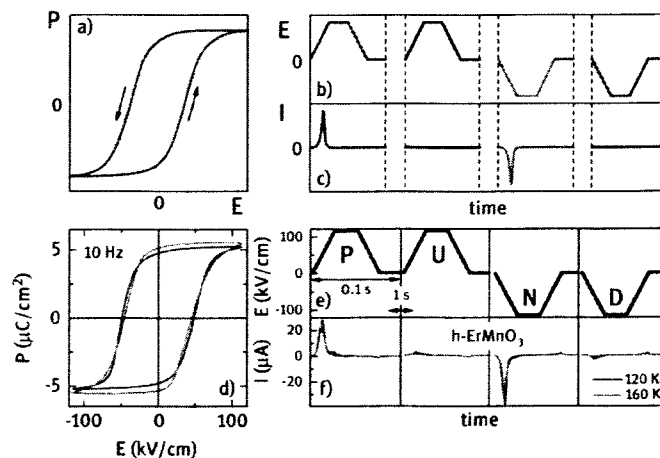

Figure 3: (a) Schematic plots of the $P(E)$ hysteresis loop as expected for a ferroelectric state. (b) and (c) Schematic plot of the applied field (a) and of the polarization-induced current response (b) as expected for a PUND measurement of a ferroelectric. Frames (d)–(f) show $P(E)$ and PUND results for h-$ErMnO_3$ [10, 12] at 120 and 160 K, which represent experimental examples corresponding to frames (a)–(c). The 160 K curve represents a measurement for which non-intrinsic effects start to contribute to the overall polarization indicated by the small peaks in the second and the forth pulses.

'An alternative to conventional $P(E)$ measurements, partly avoiding these problems, is the so-called PUND experiments. For this experimental method, a sequence of field pulses is applied to the sample, with two positive pulses followed by two negative ones as indicated in Figure 3(b). For a ferroelectric state, the monitoring of the time-dependent current $I(t)$ should reveal a response as schematically indicated in Figure 3(c). Ideally, a peak in the current should arise at the increasing flanks of the first and third pulses. This mirrors the switching of the polarization, involving the reorientation of the dipolar moments. This reorientation corresponds to a motion of charges and thus generates a current pulse. This pulse should, however, be absent at the second and forth pulses, which have the same polarity as the preceding ones. There the polarization was already switched into the same direction by the previous pulse and therefore no dipolar motion (and, thus, no current pulse) is expected. For non-intrinsic contributions to the polarization, the latter argument usually is not valid and $I(t)$ looks the same for the two succeeding pulses with same polarity. In Figure 3(d) and Figure 3(f) we show an example, h-ErMnO$_3$ [12], for a ferroelectric hysteresis loop as well as the measured current of a PUND measurement (the ferroelectric properties are discussed in detail in Section 3.2). Both experiments are performed at 120 and 160 K. For the latter, the hysteresis loop (Figure 3(d)) shows an additional non-intrinsic contribution to the polarization. This non-intrinsic effect gives rise to small peaks in the current signal of the PUND measurement (Figure 3(f)) while the second and the forth voltage pulses are applied (Figure 3(e)). Therefore, this PUND method is very useful to discriminate between intrinsic and non-intrinsic polarization effects.

Finally, we want to mention that pyrocurrent measurements also can be used to check for the occurrence of ferroelectricity. They were e.g. of key importance for the first detection of the small polarizations in spin-spiral systems like TbMnO$_3$ [15]. Usually, for these experiments the sample is cooled below its ferroelectric transition temperature under an applied high electrical field, which ideally should lead to a monodomain polar state. In a subsequent heating run without external field, the pyrocurrent is monitored. When crossing the transition, the reorientation of the dipolar moments that return to their disordered states in the paraelectric phase should lead to a pyrocurrent pulse. From the integration of this time-dependent current signal, the polarization change at the transition can be determined. When applying the prepoling field in the opposite direction, the pyrocurrent also should invert its polarity. This can be regarded as a somewhat indirect check of the switchability of the polarization, prerequisite for a true ferroelectric state. It should be noted that this method is only suited for well insulating samples. Notably, in multiferroics ferroelectric ordering can often also be triggered by applying magnetic fields. In such cases, magnetocurrent measurements can be used to detect the polarization changes at these transitions.

3 Ferroelectric signatures in various multiferroics

In the following sections, we review the ferroelectric ordering and partially the tune-ability for prominent examples of *type I* and *type II* multiferroics [14]. Ferroelectricity in type I multiferroics often originate from the lone-pair mechanism, geometrically driven effects or charge ordering. In BiFeO$_3$ [7], Bi^{3+} ions play the major role for the lone-pair mechanism featuring two outer 6s electrons not involved in chemical bonding. This "negative electron charge" gives rise to a high polarization and, in case of long-range ordered lone-pairs, leads to ferroelectricity. For this prime example of a room-temperature multiferroic system we briefly review the dielectric properties as well as the ferroelectric hysteresis loops for single crystals.

Charge-order, which is often observed in transition-metal compounds containing mixed valence ions, can result in ferroelectric ordering. Among other systems, like TbMnO$_5$ or Ca$_3$CoMnO$_6$ [55], LuFe$_2$O$_4$ [50] and the oldest known magnetic material, Fe$_3$O$_4$, are assumed to show this type of multiferroicity. We elucidate here the remarkable charge-order-driven relaxor-ferroelectric properties of Fe$_3$O$_4$.

The geometrically driven improper ferroelectricity observed, e.g. in the hexagonal manganite YMnO$_3$ [56] (as discussed in more detail in DOI:10.1515/PSR.2019.0014), is realized via a tilting of the MnO$_5$ bipyramids leading to Y displacements along the crystallographic c-direction at T_c far above ambient temperatures ($T_c > 900$ K) [11]. The antiferromagnetic ordering of the magnetic Mn^{3+} ions – for ErMnO$_3$ and YMnO$_3$ – occurs at temperatures around 80 K [57]. However, their complex ferroelectric domain patterns with topologically protected vortex structures and the fascinating functionalities arising at the domain walls put these multiferroics into the scientific focus for domain-wall-based nanoelectronics [5, 6, 58].

Another driving force for the revival of the research on multiferroics, especially those of type II (DOI:10.1515/PSR.2019.0016), was the discovery of magnetic ferroelectrics exhibiting strong magnetoelectric coupling about 15 years ago. In 2003, Kimura et al. [15] demonstrated improper ferroelectric ordering in TbMnO$_3$, which can be controlled by an external magnetic field. The revealed polarization for TbMnO$_3$ is rather low and of the order 600 µC/m^2 [15, 16]. By partially or fully replacing the Tb^{3+} ion by Dy^{3+}, the ferroelectric polarization can reach values of up to 3,000 µC/m^2. Besides these two most famous type II multiferroics, dozens of further interesting systems exist, which are discussed in detail in various reviews [14, 18, 19]. For many of

·them, the evolution of spin spirals due to frustrated magnetic order, spin-orbit coupling as well as exchange striction for collinear spin structures magnetically induces an improper ferroelectric polarization by breaking the inversion symmetry. This multiferroic mechanism is directly linked to some type of frustrated spin order, which makes them one of the most exciting developments in this research field [1, 4, 14]. The most discussed mechanism is the inverse Dzyaloshinskii–Moriya interaction or spin-current in spin-spiral systems [59–61]. For that mechanism the intensively investigated $DyMnO_3$ and $LiCuVO_4$ constitute prime examples.

3.1 Lone-pair multiferroicity in $BiFeO_3$

The functional properties, possible applications and the morphologies of multiferroic $BiFeO_3$ belonging to the rare class of materials with long-range magnetic and ferroelectric order at ambient temperatures are discussed e.g. in Ref. [62]. Here, we only briefly document the dielectric and ferroelectric properties of single crystalline $BiFeO_3$, which crystallizes (space group R3c) in a rhombohedrally distorted perovskite structure [7, 63]. The R3c symmetry allows for weak ferromagnetism as well as for spontaneous polarization along the crystallographic [111] direction. The two valence electrons of the Bi-ion, which do not participate in the chemical bonding, play a crucial role establishing the high ferroelectric polarizability leading to P values of the order of 100 $\mu C/cm^2$ [7, 64, 65]. The synthesis of large stoichiometric $BiFeO_3$ crystals turned out to be challenging. Impurities and defects can significantly impact the magnetic and dielectric properties. For the latter, impurity-induced conductivity and, thus, the formation of MW type contribution can lead to spurious effects. Moreover, the detection of intrinsic ferroelectric hysteresis loops at ambient temperatures can be hampered or even impeded due to such extrinsic contributions. Nevertheless, the overall magnetic and structural properties of $BiFeO_3$ are well characterized. The system shows polar order close to 1,100 K and antiferromagnetic ordering at about 645 K [66], which varies, most likely due to sample quality, between 595 and 650 K [67]. The displacement of Bi^{3+} and Fe^{3+} ions with respect to the ideal perovskite structure contributes to the electric polarization, which is only slightly temperature dependent [68, 69].

Figure 4 shows for various frequencies the temperature-dependent dielectric constant (a) and the conductivity (b) of a $BiFeO_3$ single crystal [64]. Distinct signatures of MW relaxations are indicated by the step-like increase of $\varepsilon' \approx 80$ (the intrinsic value at low temperatures) to an upper plateau value of about 10^4. The inset in (a) denotes an enlarged view of the temperature-dependent intrinsic dielectric constant as detected for high frequencies and temperatures below 300 K. Here, MW contributions do not play any role and no significant frequency dependence is observed. A dielectric analysis close to the ferroelectric transition at high temperature is hampered due to possible decomposition of $BiFeO_3$. However, e.g. Krainik et al. [70] tried using microwave frequencies to measure the dielectric properties up to 1,120 K. The temperature-dependent conductivity of the $BiFeO_3$ single crystal is shown in Figure 4(b). At low temperatures, it is mainly dominated by ac conductivity due to hopping charge transport. The inset presents the ac conductivity behaviour for 100 K in a broad frequency range pointing towards a super-linear power law, i.e. the frequency exponent exceeds 1. The origin of this behaviour still needs to be clarified; however, it is also rather common in transition metal oxides [71]. The temperature-dependent dc conductivity σ_{dc} corresponds to the regions where $\sigma'(T)$ becomes frequency independent, which leads to a merging of the curves for different frequencies. It behaves thermally activated with an activation energy of 0.39 eV. Finally, at high temperatures $\sigma'(T)$ deviates from the frequency-independent σ_{dc} because MW contributions start dominating the measured conductivity.
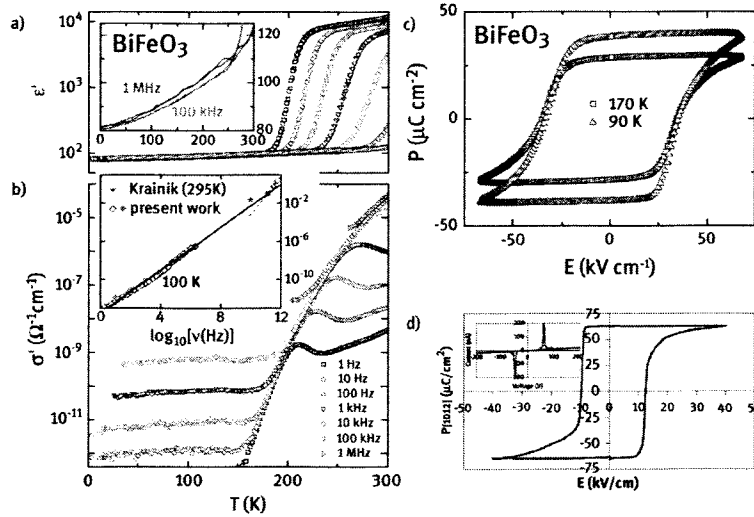
Figure 4: Temperature-dependent dielectric constant (a) and conductivity (b) for frequencies between 1 Hz and 1 MHz [64]. The inset in (a) denotes the temperature dependence of the dielectric constant as measured at 100 kHz and 1 MHz on an enlarged linear scale. The inset in (b) shows the frequency-dependent ac conductivity at 100 K [64, 70]. The solid line indicates power-law behaviour of the conductivity with a frequency exponent of 1.15. (c) Ferroelectric hysteresis loop measured at 6 Hz for 90 and 170 K [64]. (d) Ferroelectric hysteresis loop of a highly insulating $BiFeO_3$ single crystal at room temperature. The saturation polarization is in the order of 60 μCcm^{-2} and the coercive field is 12 kV/cm [65]. The inset shows the raw data of this polarization measurement. *[(a), (b) and (c) Reprinted with permission from Springer Nature, J. Lu et al., Eur. Phys. J. B 75, 451 (2010). (d) Reprinted from D. Lebeugle, D. Colson, A. Forget, and M. Viret, Appl. Phys. Lett. 91, 022907 (2007) with the permission of AIP Publishing].*

Ferroelectric hysteresis loops for that specific sample were measured at low temperatures (c.f. Figure 4(c)) [64]. For various temperatures below 200 K ferroelectric polarizations of the order of 30–40 $\mu C/cm^2$ and coercive fields around 20 kV/cm were detected, revealing typical hysteresis loops like in proper ferroelectrics. For another $BiFeO_3$ bulk single crystal, exhibiting a five decades higher room temperature resistivity, Figure 4(d) presents a ferroelectric hysteresis determined at 300 K [65]. The values of the saturation polarization (35 $\mu C/cm^2$) and the coercive field (15 kV/cm) are rather similar and finally not too far away from the theoretically predicted values as well as from those detected in thin films [7]. Finally, conductivity matters and electric-field poling seems a feasible way of controlling the ferroelectric as well as the interesting domain properties in this rare example of a room-temperature multiferroic systems. More details on the magnetoelectric and dielectric properties are described in detail in the review by Catalan and Scott [62] as well as discussed in DOI:10.1515/PSR.2019.0070.

3.2   Geometrically driven improper ferroelectricity in $RMnO_3$

Geometrically driven systems, like the hexagonal manganites $RMnO_3$ (R = In, Y, Er, Dy, Ho, ..., Lu), constitute a highly interesting class of multiferroics due to their versatile properties. Especially, the research on their complex (multi)ferroic domain structure aims at their application as functional elements in future nanoelectronics [6, 58, 72, 73]. Here, we focus on the ferroelectric properties of yttrium and erbium manganites. They display improper ferroelectricity ($T_c \approx$ 1,200–1,500 K) [74] exhibiting a cloverleaf pattern of the ferroelectric domains due to the formation of six possible domain states. The corresponding domain walls are arranged around vortex-like topological defects. At T_c, a structural transition via unit-cell tripling drives this ferroelectricity resulting in a fascinating domain pattern. An example is depicted as inset in Figure 5 revealing a vortex density of about $10^4/mm^2$ (or 0.01/μm^2). The density of the complex vortex-domain pattern depends on how the samples were cooled from temperatures above T_c [75]. The corresponding ferroelectric domains and domain walls are relatively robust as they are attached to these topologically protected vortices [76]. Beside the effect of sample preparation on the vortex density, within these constraints electric fields should be perfectly suited for manipulating the domains and domain walls. However, electric-field poling studies of hexagonal manganites are rare [9, 11, 12]. Dielectric spectroscopy performed in a broad temperature and frequency range as well as polarization measurements enable the investigation of the macroscopic polar response to applied electric fields.
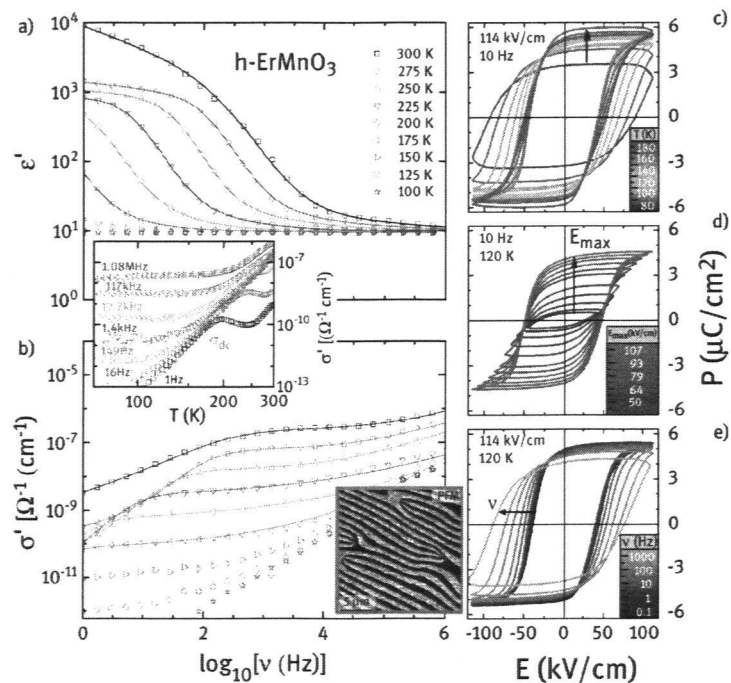
Figure 5: (a) Dielectric constant and (b) conductivity for various temperatures for a single crystalline h-ErMnO$_3$ sample oriented with out-of-plane polarization. The lines are fits with an equivalent circuit. The inset presents an Arrhenius representation of the conductivity featuring a thermally activated behaviour of the bulk dc conductivity, which is indicated by the pulse. (c) Temperature-, (d) electric field- and (e) frequency-dependent hysteresis-loop measurements. The lower inset denotes the polar surface pattern measured via piezo-response force microscopy [12]. [*A. Ruff et al. Frequency dependent polarisation switching in h-ErMnO$_3$, Appl. Phys. Lett.* **112**, *182908 (2018) used in accordance with the Creative Commons Attribution (CC BY) license*].

The detailed analysis of the dielectric properties allows determining the temperature- and frequency-dependent range for which e.g. single-crystalline h-ErMnO$_3$ exhibits purely intrinsic dielectric behaviour. So far, often extrinsic so-called MW polarizations arising e.g. from surface barrier layers, especially at ambient temperatures, have hampered field-poling measurements [77]. Insights into the polarization of hexagonal manganites were mainly gained from ferroelectric hysteresis loops recorded at fixed temperature and frequency, as well as pyrocurrent measurements [78–80]. However, many oxide materials [21, 47, 81] require – as already mentioned – a thorough dielectric investigation accompanied by an equivalent-circuit analysis. This is an appropriate way for separating the intrinsic bulk dielectric properties from extrinsic effects. For example, a thorough dielectric analysis performed for YMnO$_3$ evidenced barrier-layer capacitances arising from extrinsic effects [77]. In a recent study [12], precise dielectric analyses of h-ErMnO$_3$ have determined a regime in which intrinsic ferroelectric hysteresis loops can be clearly revealed as a function of frequency, temperature and applied electric fields. Figure 5 shows the frequency-dependent dielectric constant ε'(a) and conductivity σ'(b) of h-ErMnO$_3$ for various temperatures. Similar to the YMnO$_3$ [77], for $T > 150$ K the dielectric constant reveals a distinct frequency-dependent step-like decrease from "colossal" [48] values of up to 10^4 to intrinsic values of about 15, which is a typical signature of a MW relaxation arising at interface layers. For low temperatures ($T < 150$ K) no step-like feature remains in ε' within the measured frequency range from 1 Hz to 1 MHz. An equivalent-circuit model is used to fit the dielectric spectra (denoted by the lines in (a) and (b)) [12, 21]. From these results the contributions of the bulk and MW-type interfaces can be separated.

For high temperatures, the conductivity $\sigma'(\nu)$ (Figure 5(b)) exhibits an increase from a low conductivity to a plateau, which denotes the bulk dc conductivity σ_{dc}. For higher frequencies, the bulk conductivity shows a power-law increase, which is best revealed at low temperatures. It indicates the regime of universal dielectric response, signifying hopping conductivity [82]. The temperature dependence of σ_{dc} is denoted by the plusses in the inset of (b). Its behaviour follows an Arrhenius law with an activation energy of 0.29 ± 0.01 eV, which is in excellent agreement with previously reported values [77, 83]. Consistent with the barrier-layer framework, σ_{dc} follows the left flank of the relaxation peak arising in $\sigma'(T)$ for various frequencies. Altogether, the step-like features in the dielectric properties are indeed the typical signatures of MW relaxations. The formation of a Schottky diode constituting thin barrier layers at the sample-electrode interface seems to be the dominant

mechanism. However, also less conductive domain walls may play a crucial role, which would allow designing colossal-dielectric-constant materials via topological protected domain walls [77].

The saturation polarization for hexagonal manganites was calculated to be of the order of 5–6 $\mu C/cm^2$ [84]. As mentioned in Section 2.1, contributions from barrier-layer capacitances can superimpose intrinsic ferroelectric hysteresis loops. A proper analysis requires knowledge of the temperature and frequency range for which pure intrinsic ferroelectric switching behaviour can be detected. From the dielectric analysis of h-$ErMnO_3$, a frequency range from 0.1 Hz to 1 kHz within the temperature range from 80 to 180 K is determined for which pure intrinsic dynamic ferroelectric switching behaviour is expected to prevail. In addition, high electric activation fields E_a are required to reach saturation polarization. Figure 5 depicts well-defined hysteresis loops as function of temperature (c), electric excitation fields (d) and applied excitation frequency (e).

Ruff *et al.* [12] reported that measurements at temperatures around 120 K seem to be an ideal compromise of excluding non-intrinsic effects, which are confirmed by the absence of addition peaks in PUND measurements (c.f. Figure 6(b)), but still having achievable electric activation fields for polarization reversal. For measurements at 120 K, an excitation frequency of 10 Hz and applied fields of 114 kV/cm result in a text book-like hysteresis loop revealing good agreement with the calculated [84] saturation polarization P_s of the order of 5– 6 $\mu C/cm^2$ [12]. When the temperature exceeds 150 K, the intrinsic hysteresis loop begins to be superimposed by the aforementioned barrier layer contributions, resulting in a slightly rounded saturation polarization for the highest applied electric fields (c.f. red curves in Figure 5(c)). To reach saturation polarization, it often requires at least an E_a exceeding two times $|E_c|$, which is of the order of 40 kV/cm (c.f. Figure 5(d)). In case of reduced E_a or at lower temperatures (E_c increases with decreasing temperature), only partial polarization reversal can be achieved resulting in a reduced value of P_s. In the case of h-$ErMnO_3$ it is assumed that domain growth of the predefined topological domains (see lower inset in Figure 5, which depicts the polar surface pattern measured by piezo-response force microscopy) [9, 12] or bubble domain formation is the underlying process for polarization reversal. One hundred and twenty kelvins is also ideally suited to investigate the dynamic frequency-dependent polarization-reversal process between 0.1 Hz and 1 kHz (Figure 5(e)). The coercive field strongly increases with increasing frequency, finally leading to a partial polarization switching for $\nu > 300$ Hz. Even in the case of maximum polarization, a distinct volume fraction of "opposite" domains remains, as domain walls between two topologically protected vortices are most likely not annihilated. However, these opposite domains are constricted to narrow "channel"-like domains, especially at high electric excitation fields [85]. For decreasing absolute values of the applied fields, the "channel"-like domains split up again and two distinct domain walls develop. The remanent polarization denotes the balanced state of preferred domains versus the opposite "channel"-like domains.
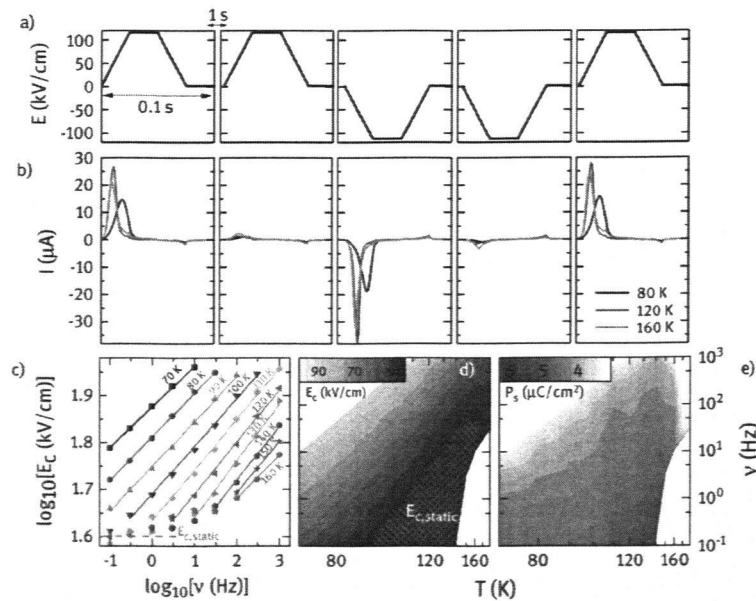
Based on these results, special emphasis is put on the frequency-dependent polarization switching, which can be explained in terms of domain-wall movement. Interestingly, this improper ferroelectric material exhibits similar behaviour compared to proper ferroelectrics, showing pure domain-wall movement [12]. But, compared to ferroelectrics, such as BaTiO$_3$, the polarization is a secondary-order parameter. The impact of this somehow "predefined" and "fixed" domain pattern on the ferroelectric switching needs to be verified.

The hysteresis results of Figure 5 can be compared to a recent study by Yang et al. [86] who calculated the dynamic hysteresis loops based on the Ginzburg–Landau theory. The measured $P(E)$ loops ($v < 300$ Hz) are in perfect agreement with those calculated using the temporal evolution of the order parameters derived from the time-dependent Ginzburg–Landau equation [12, 86]. Interestingly, these loops from theory are solely derived from movements of domain walls connecting topologically protected vortices, which provides strong evidence for pure domain-wall motion as dominating process of the polarization reversal. Further interesting features are indicated in the current response of PUND measurements performed at three different temperatures (Figure 6(a) and Figure 6(b)). The peaks arising in response to the applied first, third and fifth electric-field pulses and the virtual absence of these peaks for pulses II and IV, indeed, strongly indicate an intrinsic ferroelectric switching (c.f. Section 2.2). However, the tiny but still significant humps in the non-switching pulses can be well explained in terms of the fusion process of two domain walls at sufficiently high E_a. In this case, two domain walls are so close to each other that they form the aforementioned "channel"-like domain, which itself acts as a domain-wall-like object. Releasing the applied electrical field on a very short time scale – due to the depolarization field – results in a splitting of that object back into the two distinct domain walls. This leads to a small reduction of P_s and to a tiny current response. Hence, this peak is observable at the decreasing flank of the switching pulse and on both flanks of the non-switching pulses (Figure 6(b)). Again, this is in perfect agreement with simulations [86].

The evolution of the temperature- and frequency-dependent hysteresis loops of h-ErMnO$_3$ is discussed in terms of pure domain-wall movement. From the Kolmogorov–Avrami–Ishibashi model, Ishibashi and Orihara [87] derived a more simplified scenario with deterministic nucleation of polar domains, which is often used to describe the switching kinetics in proper ferroelectrics. Domain-wall motion is solely responsible for the polarization reversal and it only depends on the frequency of the applied field and its waveform (usually sinusoidal). Within the scope of the Ishibashi–Orihara model, the coercive field should show a simple power-law behaviour, i.e. $E_c \propto v^\beta$. For this scenario, Figure 6(c) provides an analysis of the frequency-dependent logarithm of the coercive field for various temperatures while frequency- and temperature-dependent diagrams of E_c and P_s are presented in frames (d) and (e), respectively. Linear fits yield an empirical β-exponent of about 0.103, which is of the same order as β-exponents of pure domain-wall motion in conventional ferroelectrics, like lead zirconate titanate ($\beta = 0.05$) [88] and strontium bismuth tantalate ($\beta = 0.12$) [54] as well as multiferroic domain-wall motions of LiCuVO$_4$ ($\beta = 0.08$) [89]. This constitutes another strong hint that pure domain-wall motion as proposed by Yang et al. [86] represents the major mechanism for polarization reversal in h-ErMnO$_3$. The phase diagrams shown in Figure 6(d) and Figure 6(e) demonstrate a thermally activated behaviour as well as the frequency-dependent kinetics of the domain-wall motion. This electric-field control of domain-wall motion may allow manipulating the real-space topological domain structure of hexagonal manganite.

3.3 Relaxor-ferroelectricity in magnetite

Magnetite is one of the oldest and most studied magnetic materials. Nature uses, for example, this compound in form of small crystals for the navigation of birds or magnetotactic bacteria orientating along the earth magnetic field. Altogether, the field for applications of magnetite is vast, ranging from classical applications as compass needles to magnetic recording. Besides its functionality at ambient conditions, this compound also fascinates due to its so-called Verwey transition [90, 91], which marks a metal-insulator transition at about 120 K enhancing its resistivity by at least two orders of magnitude. This is shown in Figure 7(a) where the temperature-dependent dc conductivity clearly signifies the Verwey transition, which emerges as a distinct jump in conductivity by about two orders of magnitude at 125 K. For temperatures below 200 K, an overall semiconducting behaviour is detected. Most likely, the charge ordering of Fe^{2+} and Fe^{3+}, arising from the mixed-valence state of iron ions in Fe$_3$O$_4$ (comprising one Fe^{2+}, two Fe^{3+} and four O^{2-} ions), plays a crucial role

for the unusual properties of magnetite. Interestingly, charge-order-driven ferroelectricity was proposed to explain multiferroicity in (PrCa)MnO$_3$ [92] as well as in LuFe$_2$O$_4$ [50]. For the latter compound, the charge-order mechanism is controversially debated. Thorough dielectric and ferroelectric analyses [51–53] have provided strong hints that the observed "ferroelectric polarization" is of non-intrinsic origin, i.e. MW-type relaxation, representing a typical example of a transition-metal oxide with colossal dielectric constants [21]. Hence, ferromagnetic LuFe$_2$O$_4$ most likely does not exhibit long-range polar order, thus excluding proper multiferroicity. In contrast, it seems well justified to apply the concept of charge-order-driven multiferroicity to magnetite. This was confirmed by a thorough investigation of single-crystalline magnetite using broadband dielectric spectroscopy and frequency-dependent ferroelectric polarization measurements [8]. These results point to a regime of relaxor-like polar ordering in Fe$_3$O$_4$, arising from the continuous freezing of polar degrees of freedom and the formation of a tunnelling-dominated glasslike state at low temperatures. Within this phase, for which proper long-range ferroelectricity is excluded due to its centrosymmetric monoclinic symmetry [93], indeed distinct ferroelectric hysteresis loops are revealed (Figure 7(b)). Not only single-crystalline Fe$_3$O$_4$ exhibits ferroelectric properties, but also for thin films PUND measurements have evidenced the occurrence of multiferroicity at low temperatures [94]. However, based on polarization measurements alone, there may still be some doubts concerning their intrinsic origin, as in semiconducting materials Schottky-diode-induced surface layers, like in the aforementioned LuFe$_2$O$_4$, can lead to artificial dielectric non-linearity giving rise to hysteresis-loop-like electrical behaviour [45, 46]. Ensuring an intrinsic origin of the polar properties requires a thorough dielectric characterization in a broad temperature and frequency range.
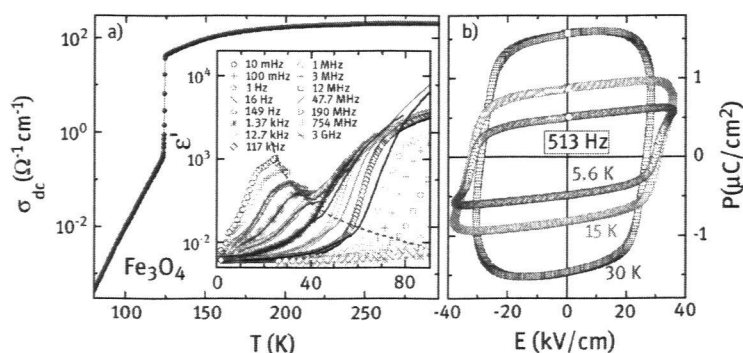

Figure 7: (a) Temperature-dependent dc conductivity for single-crystalline Fe$_3$O$_4$ [8]. The Verwey transition clearly shows up as jump in conductivity by two orders in magnitude. Inset: $\varepsilon'(T)$ of magnetite for various frequencies obtained with silver-paint (symbols) and sputtered gold contacts (solid lines). The dashed line, calculated assuming a Curie–Weiss law, illustrates the temperature dependence of ε_s of the main intrinsic relaxation. (b) Ferroelectric polarization P of Fe$_3$O$_4$ as a function of external electric field E at 513 Hz and three temperatures [8]. *[Reprinted with permission from F. Schrettle et al., Phys. Rev. B **83**, 195109 (2011). Copyright 2018 by the American Physical Society].*

The inset of Figure 7(a) depicts $\varepsilon'(T)$ at low temperatures (below the Verwey transition) for frequencies between 10^{-2} and 3×10^9 Hz. To reveal the influence of possible extrinsic Schottky layer-based effects, two different types of metal contacts were used [21]. Indeed a metal contact-related difference in dielectric properties is revealed, especially for low frequencies above 50 K, which is indicated by the discrepancy of the solid lines (sputtered gold contacts) and symbols (silver-paint contacts). $\varepsilon'(T)$ exhibits a distinct step-like feature from values of up to 10^3–10^4 down to its high-frequency limit of about $\varepsilon_\infty \approx 60$. For decreasing temperature, this step shifts to lower frequencies. For low temperatures, the dielectric spectra reveal at least three partially superimposing relaxation steps (c.f. 149 Hz curve, where their points of inflection are approximately located at 10, 30 and 50 K). One dielectric anomaly emerges as a broad maximum below 40 K; the corresponding static dielectric constant ε_s is strongly temperature-dependent as indicated by the dashed line. These are typical signatures of relaxorferroelectricity [8]. Most likely, the freezing-in of short-range clusters that are ferroelectrically ordered drives this behaviour. The mentioned strong increase of $\varepsilon_s(T)$ follows a Curie–Weiss law (dashed line in Figure 7(a)). At high temperatures, this relaxor-like feature is partially superimposed by extrinsic, electrode-dominated effects as evidenced by the disagreement of the $\varepsilon'(T)$ curves for different contact materials (symbols and lines in the inset of Figure 3). However, the relaxation feature itself is well reproduced in both measurements, clearly pointing its intrinsic nature. Moreover, even in relaxor-ferroelectrics well-developed ferroelectric hysteresis loops at low temperatures should arise. Therefore, to account for the intrinsic properties, Figure 7(b) shows ferroelectric hysteresis loops at sufficiently low temperatures (5.6, 15 and 30 K) and at a reasonable frequency of 513 Hz (Fe$_3$O$_4$ requires high electric excitation fields for poling and thus we have used a high-voltage booster, limiting the applicable frequency to the sub kHz-range). For 5.6 K, indeed a characteristic hysteresis loop is measured [8], which is further confirmed by the PUND results at 15 K of magnetite thin films [94]. Typical for relaxor-

ferroelectrics are relatively broad loops in the nearly long-range-ordered state, i.e. at low temperatures, while more narrow hystereses should be detected in the vicinity of the transition (at higher temperatures) [28]. However, the rather strong temperature-dependent increase in conductivity of the single-crystalline Fe_3O_4 sample hampered hysteresis-loop measurements for $T > 15$ K. The intrinsic ferroelectric polarization of magnetite detected at 5.6 K is about an order of magnitude lower than that in conventional ferroelectrics.

In summary, magnetite reveals the typical signature of relaxor-ferroelectricity and a continuous slowing down of its polar dynamics [8]. Most likely the loss of inversion symmetry occurs on a local scale only due to the cluster-like short-range polar order. One can assume that the polar and charge degrees of magnetite are intimately related. Hence, the charge-order should also be of short-range type and exhibit freezing at low temperatures. However, it may not reach complete arrest. Instead, an evaluation of the relaxation dynamics of magnetite rather indicates a slowly fluctuating glasslike state at low temperatures (a "charge glass"), which is dominated by quantum-mechanical tunnelling [8]. Excess heat capacity as often found for glassy materials corroborates this scenario. A possible microscopic picture is that the suppression of long-range charge order in magnetite arises from the Fe^{2+}/Fe^{3+} B-site ions sitting on a strongly frustrated pyrochlore lattice. The shown results contribute to the ongoing debate of the presence of ferroelectricity in magnetite and of the discrepancy between the theoretically expected ferroelectricity and the frequent finding of a centrosymmetric structure.

3.4   Electric-dipole-driven magnetism in a charge-transfer salt

Charge-order-driven ferroelectricity constitutes a promising way to establish multiferroic order [42]. Charge order results from strong electronic correlations. Prime examples for such a mechanism are found in various organic charge-transfer salts having effectively ¼-filled hole bands [95, 96]. Indeed, electronic ferroelectricity was found in several members of this material class [95, 96] and even multiferroicity was detected [13, 97, 98].

An interesting recent example is the antiferromagnetic quasi-two-dimensional organic charge-transfer salt κ-(BEDT-TTF)$_2$Cu[N(CN)$_2$]Cl (κ-Cl) [13]. Figure 8(a) shows a top view of the ac plane of κ-Cl revealing dimers of ET molecules with half-filled dimer bands [13, 99, 100]. Recent reports [101–103] demonstrate the importance of intra-dimer degrees of freedom and inter-site interactions. In a nutshell, within the ET layers adjacent molecules form dimers on which a single electron hole is delocalized above $T_{FE} \approx 25$ K. As proposed in Ref. [13], below T_{FE} the hole becomes localized, with its probability density being enlarged at one ET molecule of the dimer (c.f. Figure 8(a)), establishing long-range charge order (but see Ref. [104] for a contrasting view). The resulting ferroelectricity was clearly evidenced by dielectric and polarization measurements [13] as will be discussed below. Notably, κ-Cl exhibits a well-pronounced jump of the temperature-dependent conductivity close to 25 K [13, 105, 106], corroborating the occurrence of charge order at T_{FE}. At low temperatures, the hole spins constitute intralayer antiferromagnetic and interlayer ferromagnetic exchange, leading to an overall antiferromagnetic order, i.e. κ-Cl is multiferroic. As evidenced e.g. by magnetic susceptibility measurements [99, 107], at T_{FE} polar and spin order arise almost simultaneously. This was ascribed to electric-dipole-driven magnetic ordering, which is triggered by the reduction of geometrical frustration induced by the charge ordering [13]. This represents an unconventional type of multiferroic ordering where dipolar order drives spin ordering, in marked contrast to the well-known mechanism of spin-driven ferroelectricity as appearing, e.g. in LiCuVO$_4$.
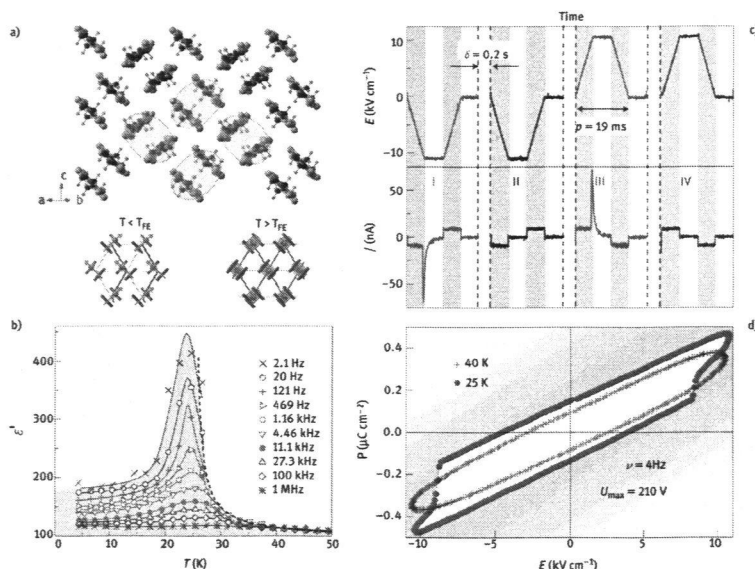
Figure 8: (a) Top view of the ac plane of κ-Cl showing the layers formed by the ET molecules [13]. In the upper part of the figure, selected dimers formed by adjacent ET molecules are highlighted by grey ellipses. The lower part of (a) schematically depicts the ac planes for temperatures below and above T_{FE}. Here the ET molecules are indicated by the thick grey lines. The red spheres denote the electron holes; for $T > T_{FE}$, the red shaded areas indicate their delocalization within the dimer. The orange arrows illustrate the dipolar moments proposed to arise below T_{FE} due to charge ordering. (b) Temperature dependence of the dielectric constant $\varepsilon'(T)$ for various frequencies measured along the b direction (solid lines are guides for the eyes) [13]. The dashed line indicates Curie–Weiss behaviour. (c) PUND measurement performed at 25 K with waiting time δ and pulse width p [13]. The upper part of the graph shows the excitation signal, the lower part the resulting time-dependent current. (d) Ferroelectric hysteresis loop measurement at temperatures below and above the ferroelectric phase transition at 4 Hz. *[Reprinted from P. Lunkenheimer et al., Nat. Mater. 11, 755 (2012)].*

The temperature-dependent dielectric constant $\varepsilon'(T)$ of κ-Cl is depicted in Figure 8(b) for various frequencies and the electrical field along the b direction. At around 25 K, well-pronounced peaks with values of ε' reaching up to several hundred are clearly revealed. Interestingly, the temperature of the peak maximum remains nearly constant for all frequencies while the amplitude strongly decreases with increasing frequencies. This is a typical behaviour of order–disorder-type ferroelectrics [26]. As discussed in Section 2.1, in this case disordered electric dipoles already exist at high temperatures and order below the phase transition at T_{FE} [25, 26], leading to an overall net polarization. For κ-Cl we assume that the electron holes at the dimers (c.f. Figure 8(a)) fluctuate between the two ET molecules at $T > T_{FE}$ and cooperatively lock-in at one of the two molecules for $T < T_{FE}$. Therefore, the polarization should primarily occur within the ac-plane. However, due to an inclined spatial orientation of the ET molecules [100], also a polarization along the b direction is induced. We found that this polarization and the corresponding peak in $\varepsilon'(T)$ are much easier to detect for the electrical field oriented along this direction. This follows from the fact that the dc charge transport along b in this material is much lower than within the ac planes [13], where it strongly hampers meaningful dielectric and polarization measurements [108].

It should be mentioned that the occurrence of CO in κ-Cl is still controversially discussed [104, 109, 110]. However, in the related systems κ-(BEDT-TTF)$_2$Hg(SCN)$_2$Cl and α-(BEDT-TTF)$_2$I$_3$, the occurrence of CO is undisputed. In the first system, very recently CO-driven ferroelectricity was clearly evidenced by length-change measurements and dielectric spectroscopy [111]. Moreover, in the α system, relaxor-ferroelectricity was reported, again based on similar mechanisms as discussed for κ-Cl above [112].

Dielectric spectroscopy alone usually is insufficient to provide a final proof of ferroelectricity [45, 46]. As discussed in Section 2.2, in addition non-linear polarization measurements should be performed, especially ferroelectric hysteresis-loop and/or PUND measurements [54]. Figure 8(c) shows the results of a PUND measurement applied to κ-Cl, for which four trapezoid pulses, preceded by a prepoling pulse (not shown), were applied to the sample [13]. The detected current signal reveals strong peak-like features occurring when the electric field exceeds about 10 kV/cm for the first and third pulses, signifying the switching of the polarization. Just as expected for proper ferroelectrics (c.f. Section 2.2), the second and forth pulses do not exhibit corresponding current features. The occurrence of ferroelectricity in κ-Cl is further confirmed by $P(E)$ measurements (Figure 8(d)), revealing the typical ferroelectric hysteresis loops in the ordered phase at $T < T_{FE}$. In contrast, above T_{FE} the elliptical shape of the $P(E)$ curve signals a linear polarization response with additional loss contributions from charge transport.

In summary, the reported experimental results provide strong evidence for ferroelectricity in κ-Cl, coinciding with the onset of magnetic ordering. Notably, the ferroelectric ordering in this system seems to be based on a primarily electronic mechanism, constituting a charge-order-driven ferroelectric state. Indeed, charge-transfer salts were considered as good candidates for multiferroics with a ferroelectric state driven by charge order [42]. Interestingly, the results point towards a multiferroicity mechanism where ferroelectric order drives the magnetic one, in marked contrast to the well-known spin-driven multiferroics. From a fundamental point of view, this and related materials [101, 111, 112] are highly interesting due to their exotic multiferroic properties. From a more applied perspective, the transition temperatures as well as the limited magnitudes of polarization make them unsuited for technical applications.

3.5 Spin-driven improper ferroelectricity in DyMnO₃

DyMnO$_3$ crystallizes in a perovskite structure when grown in a specific atmosphere [16]. At low temperatures ($T_N \approx 40$ K) and in zero magnetic fields the system shows a collinear sinusoidal spin structure [113], which locks in at $T_C \approx 20$ K into a non-collinear cycloidal spin spiral giving rise to improper ferroelectricity due to the inverse Dzyaloshinskii–Moriya interaction or spin-current mechanisms [59–61], with tilted spins S_i and S_{i+1} at neighbouring atomic sites i and $i + 1$. A prerequisite for ferroelectric ordering is the breaking of the inversion symmetry, which arises in a spin-spiral system due to this tilted spin configuration. The ferroelectric polarization follows a distinct symmetry relation in these spiral magnets:

$$\mathbf{P} \propto \mathbf{e} \times \mathbf{Q}, \tag{3}$$

where $\mathbf{Q}$ is the propagation vector of the spin spiral and $\mathbf{e} = (S_i \times S_{i+1})$ corresponds to the vector along the spiral axis, i.e. the normal vector of the spiral plane [59–61]. The tilting direction, i.e. clockwise or counterclockwise, of these two spins determine the direction of the normal vector. Even for a 1D element, like a spin spiral, a chirality-like vector can be defined. As a consequence of this "handedness" of the spin spiral, the polarization can be switched, if the modulation direction is fixed [19, 20, 89].

For DyMnO₃, the spin moments lie in the b-c plane modulating along the b-axis, which induce a ferroelectric order along the c-axis. The magnetic-field dependence of the ferroelectric ordering is a typical signature for type II multiferroics. Applying a magnetic field along different crystallographic axes causes the ferroelectric polarization vector to switch, e.g. H along b gives rise to a polarization in a direction for $H > 1$ T at 2 K. In Figure 9(a), the magnetic field-dependent dielectric constant, measured at 10 kHz and for various temperatures, reveals a peak feature indicating a paraelectric to ferroelectric transition [16]. Magnetocurrent measurements (c.f. Figure 9(b)) confirm these findings and a polarization occurs only in the presence of an applied magnetic field. For 2 K, a rather high polarization of the order of 3,000 µC/m^2 is detected in the vicinity of the ferroelectric transition. The amplitude of the polarization is temperature dependent and vanishes above the "lock-in" temperature T_C. Figure 9(c) shows the $P(E)$ behaviour at 4.2 K in zero and applied magnetic fields. Indeed, in zero magnetic fields only linear electric-field-dependent contributions are detected. However, for the switched case, which is reached by applying an external magnetic field of 6 T, a typical ferroelectric hysteresis loop establishes, confirming the saturation polarization of the order of 3,000 µC/m^2. Within the framework of a spin-spiral mechanism, the electric-field-dependent polarization indicates that two domains, with left-handed and right-handed helicity of the spin spirals, exist, which allow $\pm P_a$ keeping the spin-spiral plane and the modulation direction constant. Thus, the volume fraction of domains with different helicities of the spin spiral can be switched by an electric field. However, it should be noted that this multiferroic effect is also discussed in terms of an exchange-striction mechanism, especially at low temperatures, due to Dy-Mn interactions [114].
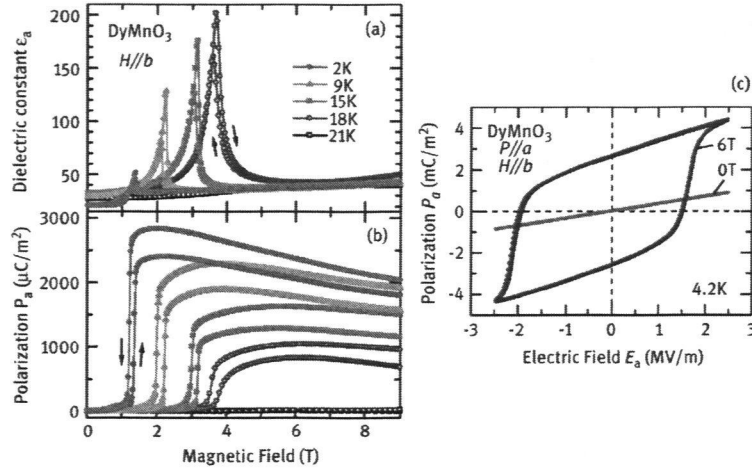
Figure 9: (a) Dielectric constant, (b) polarization and (c) $P(E)$ loops of a $DyMnO_3$ single crystal measured as function of magnetic field, which is applied along the b-axis. The dielectric constant and the polarization are detected along the a-direction for selected temperatures. The polarization loops are obtained at magnetic fields of zero and 6 T.
[Reprinted with permission from T. Kimura et al., Phys. Rev. B 71, 224425 (2005). Copyright 2018 by the American Physical Society].

3.6   Spin-driven improper ferroelectricity in the spin-½ chain cuprate system LiCuVO₄

Spin-spiral systems show the simultaneous existence and strong coupling of ferroelectric and magnetic ordering [14, 19, 59–61]. Especially, the latter allows investigating the interplay of electrical and magnetic degrees of freedom leading to complex multiferroic ordering. In this section, we focus on the multiferroic properties of a typical spin-driven ferroelectric material, the spin-½ chain cuprate $LiCuVO_4$ [17]. In general, spin-½ systems display a rich variety of exotic ground states, which often are based on competing magnetic exchange leading to frustration. One of the simplest frustrated systems is the spin-½ chain, with competing nearest and next-nearest neighbour interactions. For $LiCuVO_4$, they lead to the formation of a spin-spiral order formed in the ab plane (chiral vector **e** along c) in the 3D ordered phase below T_N of 2.5 K with the propagation along the b direction [27]. In zero magnetic fields, ferroelectric polarization is induced along the a direction [17, 27]. Applying external magnetic fields affects the orientation of the chiral vector, which above a critical field H_1 of 2.5 T aligns along the magnetic field direction. Above H_2, which is of the order of 7.5 T, the spin spiral is transformed into a modulated collinear spin structure impeding an electrical polarization according to eq. (3). As a consequence of eq. (3) and due to the fact that the chirality vector aligns with the external magnetic field, external magnetic field between 2.5 and 7.5 T can switch the direction of the electrical polarization. Results of dielectric spectroscopy in applied fields up to 9 T on a single-crystalline sample oriented along different directions nicely demonstrate this switching behaviour of the ferroelectric polarization [17, 20, 27]. Figure 10(a) and Figure 10(b) show the temperature-dependent dielectric constant in various external magnetic fields for two cases: first (Figure 10(a)), H along the c direction measuring the polarization along a direction denoting the "non-switching" case as the chiral vector remains in c direction, when exceeding H_1. Second (Figure 10(b)), H is applied along a direction while detecting the dielectric properties and thus the polarization along c. Following eq. (3), this denotes the "switching" case. Not shown is another possibility, i.e. H along the crystallographic b direction. For this case it was revealed that the polarization vanishes at H_1 [27]. Interestingly, this is indeed a spin-helix state, as the rotation of the spin spiral is in ac plane and thus both **e** and **Q** point along b. In Figure 10(a) a peak shows up in the temperature-dependent dielectric constant for various magnetic fields signalling the onset of improper ferroelectricity (Section 2.1). As discussed above, at $H > H_1$ no switching of the chiral vector is expected for H along c. Exceeding higher magnetic fields $H > H_2$, the collinear spin structure impedes an electrical polarization and the peak in the dielectric constant vanishes. Figure 10(b) shows the case of switching the polarization from the a into the c direction by applying an external magnetic field along the a direction. Even for low magnetic fields, $H < H_1$, a small peak feature is still visible at T_N, denoting a slight experimental misalignment of the sample [20]. However, for higher field, $H_1 < H < H_2$, the dielectric peak denoting the ferroelectric polarization becomes much more pronounced. This perfectly agrees with the expectation for the switching case, where the chiral vector rotates into a direction, leading to a polarization along c direction. The maxima in the temperature-dependent dielectric constants, which can be easily observed as projection onto the magnetic field-dependent plane, are close to the critical fields H_1 and H_2. As the dielectric constant is a measure for the strength of the

polarization, this experiment indicates that the polarization can be indeed switched by applying an external magnetic field, confirming previous magnetocurrent and magnetodielectric experiments [17, 27]. In addition, ferroelectric hysteresis-loop measurements and PUND studies are also feasible, pointing towards an electric-field poling of the orientation of the chiral vector and thus the switching of a counterclockwise to clockwise spin spiral and vice versa via electric fields [20, 89].
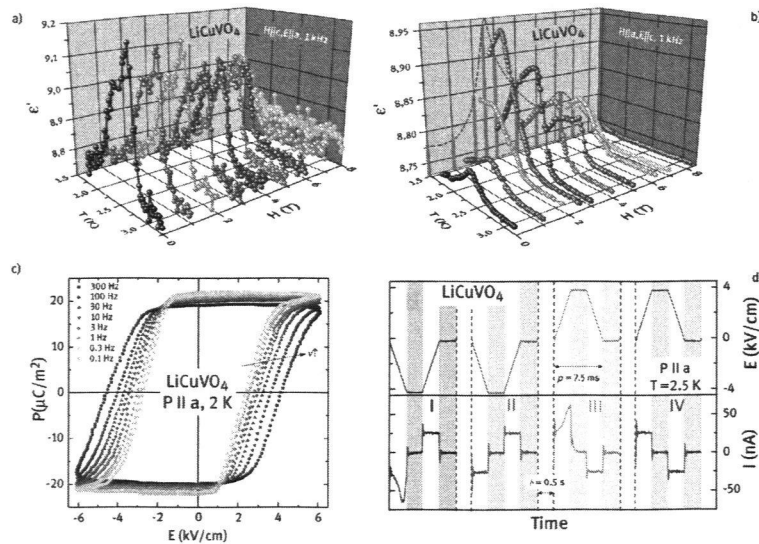

Figure 10: Dielectric constant at 1 kHz of a LiCuVO$_4$ single crystal as function of temperature and magnetic field, for (a) E along a and H along the c direction (non-switching case at $H = 2.5$ T) and (b) E along c and H along the a direction (switching case at $H = 2.5$ T) [20]. (c) Ferroelectric hysteresis loop at 2 K for various frequencies (the paraelectric background is subtracted for clarity reasons) [89]. (d) PUND measurement denoting the time-dependent excitation signal E and resulting current I for P parallel to the a direction at 2.5 K [20]. Polarization switching is evidenced by the spikes in the current response of the voltage pulses I and III as well as their absence in II and IV. *[(a), (b) and (d) Reprinted with permission from IOP Publishing, A. Ruff et al., J. Phys.: Condens. Matter **26**, 485901 (2014). (c) A. Ruff et al. Multiferroic Hysteresis Loop, Materials **10**, 1318 (2017) used in accordance with the Creative Commons Attribution (CC BY) license].*

Figure 10(c) shows a ferroelectric hysteresis-loop measurement in the ordered state at 2 K (subtracted linear paraelectric background). The frequency of the electric excitation field varies from 0.1 to 300 Hz. The revealed loop resembles the typical signature of a proper ferroelectric with a rather low saturation polarization of 20 $\mu C/m^2$, which is in the order of the theoretically predicted values [115]. The shape of the hysteresis loop smears out with increasing frequency and the coercive field increases. This feature may indicate a domain-wall movement of multiferroic domains originating from clockwise and counterclockwise spin-spiral states [89]. In Figure 10(d), results of PUND measurements at 2 K confirm the switching of the spin-driven ferroelectric polarization: additional peak features in the current responses of the first and third pulses signal switching of the macroscopic polarization. As discussed in Section 2.2, the absence of such peaks in the second and forth pulses – for theses pulses the polarization was already switched by the preceding pulse – supports the intrinsic nature of ferroelectric switching in LiCuVO$_4$. However, the underlying physical mechanism of multiferroic domains is still under debate.

In summary, the temperature and magnetic field-dependent dielectric properties of the spin-driven ferroelectric LiCuVO$_4$ were investigated in detail close to the three-dimensional ordering of its spiral magnetic structure at about 2.5 K. From these results, the switching and non-switching cases, which are expected on the basis of the theoretical symmetry predictions for multiferroic spiral magnets, are nicely confirmed. In addition, the direct observation of electric-field poling via PUND measurements demonstrates the ability to electrically control the chiral vector of the spin spiral in LiCuVO$_4$ and may indicate multiferroic domains of different helicities.

4   Conclusions and outlook

We have provided an overview of investigations of ferroelectric switching behaviour and of the dielectric properties and ferroelectric polarization in a broad temperature range as well as in applied magnetic fields for various typical multiferroic type I and type II systems. BiFeO$_3$ and hexagonal manganites are promising materi-

als for applications in domain-wall-based electronics. They bear enormous potential for a new generation of materials exhibiting tuneable domain-wall effects. Their ferroelectric properties were investigated in a broad temperature and frequency range via dielectric spectroscopy. The analysis of the detected ferroelectric hysteresis loops paves the way to manipulate the polarization of these systems and thus the ferroelectric domains by an electric field. Charge-order-driven ferroelectricity in magnetite constitutes another route for multiferroic ordering, which is more interesting from a fundamental point of view. This system reveals charge ordering, which induces relaxor-ferroelectric behaviour, solving the discrepancy between the theoretically expected ferroelectricity and the frequent finding of a centrosymmetric structure. Finally, for the type I multiferroics, we briefly reviewed the dielectric properties of the multiferroic organic charge-transfer salt, κ-Cl. The formation of charge-order-driven electronic ferroelectricity seems to be the most plausible explanation pointing to a novel mechanism of charge-order-induced magnetic ordering and coupling. This is in contrast to the well-known type II multiferroics exhibiting the spin-driven mechanism [13].

The dielectric properties of type II systems with magnetically driven ferroelectricity, exhibiting a close coupling of ferroelectric and magnetic ordering, are briefly discussed for $TbMnO_3$ and $DyMnO_3$. They show a rather high polarization as well as the magnetic control of their improper ferroelectricity. For $LiCuVO_4$, constituting a prime example for a spin-driven mechanism [19], magnetic-field-dependent studies of its dielectric properties revealed the close coupling of magnetic order and ferroelectricity. So far, only few reports address the non-linear electrically driven polarization of spin-driven multiferroics. The results of hysteresis-loop measurements at low temperatures and applied magnetic fields demonstrate the electrical-field control of the spin helicity, which can be at least partly switched from clockwise to counterclockwise or vice versa. This further corroborates the presence of (multi)ferroic domains.

There are many further examples for multiferroic compounds in literature and it is impossible to provide a detailed discussion of the polarization and dielectric properties of all of them in the present article. Very current examples are the lacunar spinels [116–119], where ferroelectricity is driven by orbital order and local electric polarization was even found to be related to the occurrence of skymions [117], small whirl-like topological spin objects which may be used for advanced types of data storage devices.

However, for all these materials it turned out that the conductivity is of utmost importance for measuring and manipulating the polar properties on a macroscopic and microscopic level, respectively. The fascinating polar properties of a broad variety of magnetoelectric and multiferroic systems allow to envisage novel functionalities and may pave the way to the development of multifunctional magnetoelectrics for applications in novel electronic devices.

Funding

References

[1] Fiebig M. Revival of the magnetoelectric effect. J Phys D Appl Phys. 2005;38:R123.

[2] Hill NA. Why are there so few magnetic ferroelectrics? J Phys Chem B. 2000;104:66–94.

[3] Eerenstein W, Mathur ND, Scott JF. Multiferroic and magnetoelectric materials. Nature. 2006;442:759.

[4] Fiebig M, Lottermoser T, Meier D, Trassin M. The evolution of multiferroics. Nat Rev Mater. 2016;1:16046.

[5] Catalan G, Seidel J, Ramesh R, Scott JF. Domain wall nanoelectronics. Rev Mod Phys. 2012;84:119.

[6] Meier D. Functional domain walls in multiferroics. J Phys Condens Matter. 2015;27:463003.

[7] Wang J, Neaton JB, Zheng H, Nagarajan V, Ogale SB, Liu B, et al. Epitaxial BiFeO₃ multiferroic thin film heterostructures. Science. 2003;299:1719.

[8] Schrettle F, Krohns S, Lunkenheimer P, Brabers VAM, Loidl A. Relaxor ferroelectricity and the freezing of short-range polar and charge order in magnetite. Phys Rev B. 2011;83:195109.

[9] Choi T, Horibe Y, Yi HT, Choi YJ, Wu W, Cheong S-W. Insulating interlocked ferroelectric and structural antiphase domain walls in multiferroic YMnO₃. Nat Mater. 2010;9:253.

[10] Ruff A, Li Z, Schafnitzel M, Krohns S, Dielectric properties and resource criticality aspects of hexagonal manganite. Ceramic Transactions. Volume 264. Proceedings of the 12th pacific rim conference on ceramic and glass technology 2018.

[11] Lilienblum M, Lottermoser T, Manz S, Selbach SM, Cano A, Fiebig M. Ferroelectricity in the multiferroic hexagonal manganites. Nat Phys. 2015;11:1070.

[12] Ruff A, Li Z, Loidl A, Schaab J, Fiebig M, Cano A, et al. Frequency dependent polarisation switching in h-ErMnO₃. Appl Phys Lett. 2018;112:182908.

*[13] Lunkenheimer P, Müller J, Krohns S, Schrettle F, Loidl A, Hartmann B, et al. Multiferroicity in an organic charge-transfer salt that is suggestive of electric-dipole-driven magnetism. Nat Mater. 2012;11:755.

[14] Khomskii D. Classifying multiferroics: mechanisms and effects. Physics. 2009;2:20.

[15] Kimura T, Goto T, Shintani H, Ishizaka K, Arima T, Tokura Y. Magnetic control of ferroelectric polarization. Nature. 2003;426:55.

[16] Kimura T, Lawes G, Goto T, Tokura Y, Ramirez AP. Magnetoelectric phase diagrams of orthorhombic $RMnO_3$ (R = Gd, Tb, and Dy). Phys Rev B. 2005;71:224425.

[17] Naito Y, Sato K, Yasui Y, Kobayashi Y, Kobayashi Y, Sato M. Ferroelectric transition induced by the Incommensurate magnetic ordering in $LiCuVO_4$. J Phys Soc Jpn. 2007;76:023708.

[18] Kimura T. Spiral magnets as magnetoelectrics. Annu Rev Mater Res. 2007;37:387.

[19] Tokura Y, Seki S. Multiferroics with spiral spin orders. Adv Mater. 2010;22:1554.

[20] Ruff A, Krohns S, Lunkenheimer P, Prokofiev A, Loidl A. Dielectric properties and electrical switching behavior of the spin-driven multiferroic $LiCuVO_4$. J Phys Condens Matter. 2014;26:485901.

[21] Lunkenheimer P, Krohns S, Riegg S, Ebbinghaus SG, Reller A, Loidl A. Colossal dielectric constant in transition-metal oxides. Eur Phys J Spec Top. 2009;180:61.

[22] Devonshire AF. Theory of ferroelectrics. Adv Phys. 1954;3:85.

[23] Cochran W. Crystal stability and the theory of ferroelectricity. Adv Phys. 1960;9:387.

[24] Jona F, Shirane G. Ferroelectric crystals. London: Pergamon Press, 1962.

[25] Blinc R, Zeks B. Soft modes in ferroelectrics and antiferroelectrics. Amsterdam: North Holland Publishing, 1974.

[26] Lines ME, Glass AM. Principles and applications of ferroelectrics and related materials. Clarendon: Oxford, 1977.

[27] Schrettle F, Krohns S, Lunkenheimer P, Hemberger J, Büttgen N, Krug von Nidda H-A, et al. Switching the ferroelectric polarization by external magnetic fields in the spin = 1/2 chain cuprate $LiCuVO_4$. Phys Rev B. 2008;77:144101.

[28] Cross LE. Relaxor ferroelectrics. Ferroelectrics. 1987;76:241.

[29] Samara GA. The relaxational properties of compositionally disordered ABO3 perovskites. J Phys Condens Matt. 2003;15:R367.

[30] Smolenski GA, Isupov VA, Agranovskaya AI, Popov SN. Ferroelectris with diffuse phase transitions. Sov Phys Solid State. 1961;2:2584.

[31] Lunkenheimer P, Schneider U, Brand R, Loidl A. Glassy dynamics. Contemp Phys. 2000;41:15.

[32] Viehland D, Jang SJ, Cross LE, Wuttig M. Freezing of the polarization fluctuations in lead magnesium niobate relaxors. J Appl Phys. 1990;68:2916.

[33] Levstik A, Kutnjak Z, Filipič C, Pirc R. Glassy freezing in relaxor ferroelectric lead magnesium niobate. Phys Rev B. 1998;57:11204.

[34] Glazounov AE, Tagantsev AK. Direct evidence for Vögel–fulcher freezing in relaxor ferroelectrics. Appl Phys Lett. 1998;73:856.

[35] Lunkenheimer P, Kastner S, Köhler M, Loidl A. Temperature development of glassy -relaxation dynamics determined by broadband dielectric spectroscopy. Phys Rev E. 2010;81:051504.

[36] Sillescu H. Heterogeneity at the glass transition: a review. J Non-Cryst Solids. 1999;243:81.

[37] Ediger MD. Spatially heterogeneous dynamics in supercooled liquids. Annu Rev Phys Chem. 2000;51:99.

[38] Cole KS, Cole RH. Dispersion and absorption in dielectrics I. Alternating current characteristics. J Chem Phys. 1941;9:341.

[39] Davidson DW, Cole RH. Dielectric relaxation in glycerine. J Chem Phys. 1950;18:1417.

[40] Havriliak S, Negami S. A complex plane analysis of -dispersions in some polymers. J Polym Sci C. 1966;14:99.

[41] Viehland D, Jang SJ, Cross LE, Wuttig M. Deviation from curie-weiss behavior in relaxor ferroelectrics. Phys Rev B. 1992;46:8003.

[42] van Den Brink J, Khomskii D. Multiferroicity due to charge ordering. J Phys Condens Matter. 2008;20:434217.

[43] Lunkenheimer P, Bobnar V, Pronin AV, Ritus AI, Volkov AA, Loidl A. Origin of apparent colossal dielectric constants. Phys Rev B. 2002;66:052105.

[44] Emmert S, Wolf M, Gulich R, Krohns S, Kastner S, Lunkenheimer P, et al. Electrode polarization effects in broadband dielectric spectroscopy. Eur Phys J B. 2011;83:157.

[45] Scott JF. Ferroelectrics go bananas. J Phys Condens Matter. 2008;20:021001.

[46] Loidl A, Krohns S, Hemberger J, Lunkenheimer P. Bananas go paraelectric. J Phys Condens Matter. 2008;20:191001.

[47] Homes CC, Vogt T, Shapiro SM, Wakimoto S, Ramirez AP. Optical response of high-dielectric-constant perovskite-related oxide. Science. 2001;293:673.

[48] Lunkenheimer P, Fichtl R, Ebbinghaus SG, Loidl A. Non-intrinsic origin of the colossal dielectric constants in $CaCu_3Ti_4O_{12}$. Phys Rev B. 2004;70:172102.

[49] Dittl A, Krohns S, Sebald J, Schrettle F, Hemmida M, Krug von Nidda H-A, et al. On the magnetism of $Ln_{2/3}Cu_3Ti_4O_{12}$ (Ln = lanthanide). Eur Phys J B. 2011;79:391.

[50] Ikeda N, Ohsumi H, Ohwada K, Ishii K, Inami T, Kakurai K, et al. Ferroelectricity from iron valence ordering in the charge-frustrated system $LuFe_2O_4$. Nature. 2005;436:1136.

[51] Ren P, Yang Z, Zhu WG, Huan CHA, Wang L. Origin of the colossal dielectric permittivity and magnetocapacitance in $LuFe_2O_4$. J Appl Phys. 2011;109:074109.

[52] Niermann D, Waschkowski F, de Groot J, Angst M, Hemberger J. Dielectric properties of charge-ordered $LuFe_2O_4$ revisited: the apparent influence of contacts. Phys Rev Lett. 2012;109:016405.

[53] Ruff A, Krohns S, Schrettle F, Tsurkan V, Lunkenheimer P, Loidl A. Absence of polar order in $LuFe_2O_4$. Eur Phys J B. 2012;85:290.

[54] Scott JF. Ferroelectric memories, 1st ed. Springer Press: Berlin/Heidelberg, Germany, 2000.

[55] Choi YJ, Yi HT, Lee S, Huang Q, Kiryukhin V, Cheong S-W. Ferroelectricity in an ising chain magnet. Phys Rev Lett. 2008;100:047601.

[56] Van Aken BB, Palstra TTM, Filippetti A, Spaldin NA. The origin of ferroelectricity in magnetoelectric $YMnO_3$. Nat Mater. 2004;3:164.

[57] Iwara N, Kohn K. Magnetoelectric effect and rare earth magnetic ordering of $ErMnO_3$. Ferroelectrics. 1998;219:161.

[58] Schaab J, Skjaervo SH, Krohns S, Dai X, Holtz M, Cano A, et al. Electrical half-wave rectification at improper ferroelectric domain walls. Nat Nano. 2018;13:1028.

[59] Mostovoy M. Ferroelectricity in spiral magnets. Phys Rev Lett. 2006;96:067601.

[60] Sergienko IA, Dagotto E. Role of the dzyaloshinskii–moriya interaction in multiferroic perovskites. Phys Rev B. 2006;73:094434.

[61] Katsura H, Nagaosa N, Balatsky AV. Spin current and magnetoelectric effect in noncollinear magnets. Phys Rev Lett. 2005;95:057205.

[62] Catalan G, Scott JF. Physics and applications of bismuth ferrite. Adv Mater. 2009;21:2463.

[63] Moreau JM, Michel C, Gerson R, James WJ. Ferroelectric BiFeO3 X-ray and neutron diffraction study. J Phys Chem Sol. 1971;32:1315.

[64] Lu J, Schmidt M, Günther A, Schrettle F, Mayr F, Krohns S, et al. Magnetic susceptibility, heat capacity, electric polarization and dielectric constants of single crystalline $BiFeO_3$. Eur Phys J B. 2010;75:451.

[65] Lebeugle D, Colson D, Forget A, Viret M. Very large spontaneous electric polarization in $BiFeO_3$ single crystals at room temperature and its evolution under cycling fields. Appl Phys Lett. 2007;91:022907.

[66] Smith RT, Achenbach GD, Gerson R, James WJ. Dielectric properties of solid solutions of $BiFeO_3$ with $Pb(Ti,Zr)O_3$ at high temperature and high frequency. J Appl Phys. 1968;39:70.

[67] Fischer P, Polomska M, Sosnowska I, Szymanski M. Temperature dependence of the crystal and magnetic structures of $BiFeO_3$. J Phys C Solid State Phys. 1931;13:1980.

[68] Palewicz A, Przenioslo R, Sosnowska I, Hewat AW. Atomic displacements in $BiFeO_3$ as a function of temperature: neutron diffraction study. Acta Cryst B. 2007;63:537.

[69] Palewicz A, Sosnowska I, Przenioslo R, Hewat AW. $BiFeO_3$ crystal structure at low temperatures. Acta Phys Pol A. 2010;117:296.

[70] Krainik NN, Khuchua NP, Zhdanova VV, Evseev VA. Phase transitions in $BiFeO_3$. Sov Phys Solid State. 1966;8:654.

[71] Lunkenheimer P, Loidl A. Response of disordered matter to electromagnetic fields. Phys Rev Lett. 2003;91:207601.

[72] Meier D, Seidel J, Cano A, Delaney K, Kumagai Y, Mostovoy M, et al. Anisotropic conductance at improper ferroelectric domain walls. Nat Mater. 2012;11:284.

[73] Schaab J, Cano A, Lilienblum M, Yan Z, Bourret E, Ramesh R, et al. Optimization of electronic domain-wall properties by aliovalent cation substitution. Adv Electron Mater. 2016;2:1500195.

[74] Lorenz B. Hexagonal Manganites—(rMnO₃): class (I) Multiferroics with strong coupling of magnetism and ferroelectricity. ISRN Cond Mat Phys. 2013;497073:2013.

[75] Griffin SM, Lilienblum M, Delaney KT, Kumagai Y, Fiebig M, Spaldin NA. Scaling behavior and beyond equilibrium in the hexagonal manganites. Phys Rev X. 2012;2:041022.

[76] Holtz ME, Shapovalov K, Mundy JA, Chang CS, Yan Z, Bourret E, et al. Topological defects in hexagonal manganites: inner structure and emergent electrostatics. Nano Lett. 2017;17:5883.

[77] Ruff E, Krohns S, Lilienblum M, Meier D, Fiebig M, Lunkenheimer P, et al. Conductivity contrast and tunneling charge transport in the vortex-like ferroelectric domain patterns of multiferroic hexagonal $YMnO_3$. Phys Rev Lett. 2017;118:036803.

[78] Adem U, Mufti N, Nugroho AA, Catalan G, Nohed B, Palstra TTM. Dielectric relaxation in $YMnO_3$ single crystals. J Alloy Compd. 2015;638:228.

[79] Dey P, Natha TK, Nanda Goswami ML. Room temperature ferroelectric and ferromagnetic properties of multiferroics composites. Appl Phys Lett. 2007;90:162510.

[80] Ismailzade I, Kizhaev SA. DETERMINATION OF THE CURIE POINT OF THE FERROELECTRICS $YMnO_3$ AND $YbMnO_3$. Sov Phys Solid State. 1965;7:298.

[81] Krohns S, Lunkenheimer P, Ebbinghaus SG, Loidl A. Broadband dielectric spectroscopy on single-crystalline and ceramic $CaCu_3Ti_4O_{12}$. Appl Phys Lett. 2007;91:022910.

[82] Jonscher AK. The 'universal' dielectric response. Nature. 1977;267:673.

[83] Holstad TS, Evans DM, Ruff A, Smabraten DR, Schaab J, Tzschaschel C, et al. Electronic bulk and domain wall properties in B-Site doped hexagonal $ErMnO_3$. Phys Rev B. 2018;97:085143.

[84] Fennie CJ, Rabe KM. Ferroelectric transition in $YMnO_3$ from first principles. Phys Rev B. 2005;72:100103.

[85] Han MG, Zhu Y, Wu L, Aoki T, Volkov V, Wang X, et al. Ferroelectric switching dynamics of topological vortex domains in a hexagonal manganite. Adv Mater. 2013;25:2415.

[86] Yang KL, Zhang Y, Zheng SH, Lin L, Yan ZB, Liu J-M, et al. Electric field driven evolution of topological domain structure in hexagonal manganites. Phys Rev B. 2017;96:144103.

[87] Ishibashi Y, Orihara H. A theory of DE hysteresis loop. Integr Ferroelectr. 1995;9:57.

[88] Scott JF, Ross FM, Paz de Araujo CA, Scott MC, Huffman M. Structure and device characteristics of $SrBi_2Ta_2O_9$-based nonvolatile random-access memories. MRS Bull. 1996;21:33.

[89] Ruff A, Loidl A, Krohns S. Multiferroic Hysteresis loop. Mater. 2017;10:1318.

[90] Verwey EJW, Haayman PW. Electronic conductivity and transition point of magnetite Fe_3O_4. Physica. 1941;8:979.

[91] Verwey EJW, Haayman PW, Romeijn FC. Physical properties and cation arrangement of oxides with spinel structures II. electronic conductivity. J Chem Phys. 1947;15:181.

[92] Lopes AML, Araujo JP, Amaral VS, Correia JG, Tomioka Y, Tokura Y. New phase transition in the $Pr_{1-x}Ca_xMnO_3$ SYstem: evidence for electrical polarization in charge ordered manganites. Phys Rev Lett. 2008;100:155702.

[93] Wright JP, Attfield JP, Radaelli PG. Long range charge ordering in magnetite below the verwey transition. Phys Rev Lett. 2001;87:266401.

[94] Alexe M, Ziese M, Hesse D, Esquinazi P, Yamauchi K, Fukushima T, et al. Ferroelectric switching in multiferroic magnetite (Fe_3O_4) thin films. Adv Mater. 2009;21:4452.

[95] Tomić S, Dressel M. Ferroelectricity in molecular solids: a review of electrodynamic properties. Rep Prog Phys. 2015;78:096501.

[96] Lunkenheimer P, Loidl A. Dielectric spectroscopy on organic charge-transfer salts. J Phys Condens Matter. 2015;27:373001.

[97] Yoshimi K, Seo H, Ishibashi S, Brown SE. Tuning the magnetic dimensionality by charge ordering in the molecular TMTTF salts. Phys Rev Lett. 2012;108:096402.

[98] Giovannetti G, Nourafkan R, Kotliar G, Capone M. Correlation-driven electronic multiferroicity in $TMTTF_2$ − X organic crystals. Phys Rev B. 2015;91:125130.

[99] Kanoda K. Mott Transition and Superconductivity in Q2D Organic Conductors, chapter 22. In: Lebed A, editor. The physics of organic superconductors and conductors. Springer: Berlin, 2008:623–642.

[100] Toyota N, Lang M, Müller J. Low-dimensional molecular metals. Berlin: Springer, 2007.

[101] Abdel-Jawad M, Terasaki I, Sasaki T, Yoneyama NN, Kobayashi N, Uesu Y, et al. Anomalous dielectric response in the dimer Mott insulator κ-(BEDT-TTF)$_2$Cu$_2$(CN)$_3$. Phys Rev B. 2010;82:125119.

[102] Hotta C. Quantum electric dipoles in spin-liquid dimer Mott insulator κ-(ET)$_2$Cu$_2$(CN)$_3$. Phys Rev B. 2010;82:241104(R).

[103] Li H, Clay RT, Mazumdar S. The paired-electron crystal in the two-dimensional frustrated quarter-filled band. J Phys Condens Matter. 2010;22:272201.

[104] Sedlmeier K, Elsässer S, Neubauer D, Beyer R, Wu D, Ivek T, et al. Absence of charge order in the dimerized κ-phase BEDT-TTF salts. Phys Rev B. 2012;86:245103.

[105] Dressel M, Grüner G, Carlson KD, Wang HH, Williams JM. Studies of the microwave resistivity of κ-(BEDT-TTF)$_2$Cu[N(CN)$_2$]Cl. Synth Met. 1995;70:927.

[106] Ito H, Ishiguro T, Kubota M, Saito G. Metal-nonmetal transition and superconductivity localization in the two-dimensional conductor κ-(BEDT-TTF)$_2$Cu[N(CN)$_2$]Cl under pressure. J Phys Soc Jpn. 1996;65:2987.

[107] Miyagawa K, Kawamoto A, Nakazawa Y, Kanoda K. Antiferromagnetic ordering and spin structure in the organic conductor, κ-(BEDT-TTF)$_2$Cu[N(CN)$_2$]Cl. Phys Rev Lett. 1995;75:1174.

[108] Pinterić M, Miljak M, Biškup N, Milat O, Aviani I, Tomić S, et al. Magnetic anisotropy and low-frequency dielectric response of weak ferromagnetic phase in κ-(BEDT-TTF)$_2$Cu[N(CN)$_2$]Cl, where BEDT-TTF is Bis(ethylenedithio)tetrathiafulvalene. Eur Phys J B. 1999;11:217.

[109] Tomić S, Pinterić M, Ivek T, Sedlmeier K, Beyer R, Wu D, et al. Magnetic ordering and charge dynamics in κ-(BEDT-TTF)$_2$Cu[N(CN)$_2$]Cl. J Phys Condens Matter. 2013;25:436004.

[110] Lang M, Lunkenheimer P, Müller J, Loidl A, Hartmann B, Hoang NH, et al. Multiferroicity in the Mott Insulating Charge-Transfer Salt κ − (BEDT − TTF)$_2$Cu[N(CN)$_2$]Cl. IEEE Trans Magn. 2014;50:2700107.

[111] Gati E, Fischer JKH, Lunkenheimer P, Zielke D, Köhler S, Kolb F, et al. Evidence for electronically driven ferroelectricity in a strongly correlated dimerized BEDT-TTF molecular conductor. Phys Rev Lett. 2018;120:247601.

[112] Lunkenheimer P, Hartmann B, Lang M, Müller J, Schweitzer D, Krohns S, et al. Electronic relaxor ferroelectricity in charge-ordered -(BEDT-TTF)$_2$I$_3$. Phys Rev B. 2015;91:245132.

[113] Kimura T, Ishihara S, Shintani H, Arima T, Takahashi KT, Ishizaka K, et al. Distorted perovskite with e^1_g configuration as a frustrated spin system. Phys Rev B. 2003;68:060403(R).

[114] Wang HW, Li CL, Yuan SL, Wang JF, Lu CL, Liu J-M. The crucial role of Mn spiral spin order in stabilizing the Dy−mn exchange striction in multiferroic DyMnO$_3$. Phys Chem Chem Phys. 2017;19:3706.

[115] Xiang HJ, Whangbo M-H. Density-functional characterization of the multiferroicity in spin spiral chain cuprates. Phys Rev Lett. 2007;99:257203.

[116] Singh K, Simon C, Cannuccia E, Lepetit M-B, Corraze B, Janod E, et al. Orbital-ordering-driven multiferroicity and magnetoelectric coupling in GeV$_4$S$_8$. Phys Rev Lett. 2014;113:137602.

[117] Ruff E, Widmann S, Lunkenheimer P, Tsurkan V, Bordács S, Kézsmárki I, et al. Multiferroicity and skyrmions carrying electric polarization in GaV$_4$S$_8$. Sci Adv. 2015;1:e1500916.

[118] Ruff E, Butykai A, Geirhos K, Widmann S, Tsurkan V, Stefanet E, et al. Polar and magnetic order in GaV$_4$Se$_8$. Phys Rev B. 2017;96:165−119.

[119] Geirhos K, Krohns S, Nakamura H, Waki T, Tabata Y, Kézsmárki I, et al. Orbital-order driven ferroelectricity and dipolar relaxation dynamics in multiferroic GaMo$_4$S$_8$. Phys Rev B. 2018;98:224306.